Published in final edited form as:
J Comp Neurol. 2010 November 15; 518(22): 4546–4566. doi:10.1002/cne.22477.

Quantitative Analysis of the Bilateral Brainstem Projections from the Whisker and Forepaw Regions in Rat Primary Motor Cortex

Kevin D. Alloway[1], **Jared B. Smith**[1], and **Kyle J. Beauchemin**[2]

[1]Department of Neural & Behavioral Sciences, Pennsylvania State University College of Medicine, Hershey, Pennsylvania 17033-2255

[2]IGERT Program in Functional Genomics, School of Biomedical Sciences, University of Maine, Orono, ME 04469, USA

Abstract

The whisker region in rat primary motor (MI) cortex projects to several brainstem regions, but the relative strength of these projections has not been characterized. We recently quantified the MI projections to bilateral targets in the forebrain (Alloway et al., 2009), and the present study extends those findings by quantifying the MI projections to bilateral targets in the brainstem. We found that both the whisker and forepaw regions in MI project most strongly to the basal pons and superior colliculus. While the MI forepaw region projects mainly to the ipsilateral basilar pons, the MI whisker region has significantly more connections with the contralateral side. This bilateral difference suggests that corticopontine projections from the MI whisker region may have a role in coordinating bilateral whisker movements. Anterograde tracer injections in MI did not reveal any direct projections to the facial nucleus, but retrograde tracer injections in the facial nucleus revealed some labeled neurons in MI cortex. The number of retrogradely-labeled neurons in MI, however, was dwarfed by a much larger number of labeled neurons in the superior colliculus and other brainstem regions. Together, our anterograde and retrograde tracing results indicate that the superior colliculus provides the most effective route for transmitting information from MI to the facial nucleus.

Indexing terms

anterograde tracing; corticopontine; corticoreticular; corticotectal; facial nucleus; motor control; retrograde labeling

Many rodents, including rats and mice, display repetitive bilateral sweeping movements of the whiskers while exploring their environment (Welker, 1964; Rice, 1995; Gao et al., 2001; Sachdev et al., 2003; Sellien et al., 2005). These rhythmic movements consist of protractions and retractions mediated by three sets of muscles (Hill et al., 2008). Each whisking cycle is initiated by contractions of the rostral-lying musculus nasalis, which pulls the whisker pad forward. Contractions of the intrinsic sling muscles rapidly pivot the whiskers further forward to produce the full extent of whisker protraction. During retraction, the nasalis and sling muscles relax while two caudal-lying muscles, the nasolabialis and maxillolabialis, contract to pull the whisker pad backward. Neuronal tracing and physiological stimulation studies indicate that the lateral facial nucleus contains most of the motoneurons that control these muscles (Klein and Rhoades, 1985; Semba and Egger, 1986; Herfst and Brecht, 2008).

Correspondence to: Dr. Kevin D. Alloway, Neural & Behavioral Sciences, H109, Hershey Medical Center, 500 University Dr., Hershey, PA 17033-2255, kda1@psu.edu.
Associate Editor: Dr. Joseph L. Price

While the kinematics of whisker movements (e.g., amplitude, frequency, whisking phase) vary substantially across different behavioral situations, most whisking behavior is characterized by some degree of bilateral coordination. Exploratory whisking is often marked by epochs (1-2s) of bilaterally-symmetric movements in which whiskers on both sides of the head move synchronously at similar amplitudes and frequencies (Gao et al., 2001; Sachdev et al., 2003; Sellien et al., 2005). During horizontal head movements, whisking movements on the two sides of the head differ in their phase relations, but may continue at the same frequency (Towal and Hartmann, 2006). In response to unilateral contacts with external stimuli, the whiskers on both sides of the head move rhythmically at similar frequencies but at different amplitudes (Sachdev et al., 2003; Mitchinson et al., 2007). This bilateral decoupling of specific kinematic features suggests that whisking is mediated by a network of interactive brain regions, each of which performs a specific computation that is modulated as new sensory information becomes available. Furthermore, the bilateral coordination evident in different types of whisking behavior indicates that interhemispheric connections are an important part of this neural network.

Several facts suggest that MI cortex and its efferent connections comprise an important part of the neural network that regulates whisking behavior and its bilateral coordination. Support for this view comes from early mapping studies showing that brief trains (<300 ms) of intracranial microstimulation (ICMS) may evoke twitches of the contralateral or ipsilateral whiskers (Hall and Lindholm, 1974; Donoghue and Wise, 1982; Gioanni and Lamarche, 1985; Neafsey et al., 1986). More recent work has shown that prolonged (1,000 ms) stimulation of MI evokes oscillatory (5–15 Hz) movements that resemble the rhythmic patterns of exploratory whisking (Berg and Kleinfeld, 2003; Haiss and Schwartz, 2005; Cramer and Keller, 2006). In addition, unilateral ablation of MI cortex disrupts bilateral synchrony and other kinematic features of whisking behavior (Gao et al., 2003).

Many tracing studies have documented the interhemispheric connections of MI cortex. The MI whisker regions in each hemisphere are interconnected by callosal projections (Porter and White, 1983, 1984; Donoghue and Parham, 1983; Reep et al., 1987; Miyashita et al., 1994;Veinante and Deschenes, 2003), and MI projects bilaterally to the thalamus, neostriatum, and claustrum (Molinari et al., 1985; Wilson, 1986, 1987; Rouiller et al., 1991; Reiner et al., 2003; Reep et al. 2008; Alloway et al., 2008; 2009). These findings have prompted the view that each set of interhemispheric projections from MI may contribute to a specific aspect of bilateral whisker coordination (Gao et al., 2003; Alloway et al., 2009).

Our lab recently analyzed the forebrain projections from both the whisker and forelimb regions in MI (Alloway et al., 2008; 2009). We compared these MI regions because forelimb movements have many degrees of freedom and, in contrast to the bilateral coordination that characterizes most whisking movements, the forelimbs are more likely to move independently. Consistent with these functional distinctions, the MI forelimb region has fewer interhemispheric forebrain connections than the MI whisker region (Alloway et al., 2009; Colechio and Alloway, 2009).

The present study extends this work by comparing the brainstem projections from these MI regions. While several reports have described MI projections to the superior colliculus (SC), the basal pontine nuclei (PN), the deep mesencephalic nucleus (DpM), and the reticular formation (Weisendanger and Weisendanger, 1982; Reep et al., 1987; Miyashita et al., 1994; Hattox et al., 2002; Leergaard et al., 2004), these studies did not compare the projections from the whisker and forepaw regions in MI. If some brainstem regions receive bilateral projections from the MI whisker but not the MI forepaw region, these target areas would be implicated in the bilateral coordination of whisking behavior. Furthermore, while some work indicates that MI projects directly to the facial nucleus (Grinevich et al., 2005), other studies

have not observed this pathway (Miyashita et al., 1994; Hattox et al., 2002). Therefore, we quantitatively compared the brainstem projection patterns in rats used previously in our analysis of MI forebrain projections (Alloway et al., 2009). To insure that tracer transport and labeling were optimal for revealing potential projections to the facial nucleus, we analyzed only those cases in which the MI tracer injections produced the greatest amount of brainstem labeling. As a further test of this hypothesis, we also injected retrograde tracers directly into the lateral facial nucleus and then searched for labeled neurons in MI cortex.

MATERIALS AND METHODS

All surgeries and neuronal tracer injections were performed on adult, male Sprague-Dawley rats according to NIH guidelines, and the procedures were approved by our Institutional Animal Care and Use Committee. Most results were obtained from rats in a previous study in which anterograde tracers were injected into MI (Alloway et al., 2009), but some results were obtained from a new set of rats that received retrograde tracers in the facial nucleus. In all cases, each rat received intramuscular (IM) injections of ketamine (20 mg/kg) and xylazine (6 mg/kg) followed by atropine methyl nitrate (0.05 mg/kg, IM), chloramphenicol (50 mg/kg, IM), and dexamethasone sodium phosphate (5 mg/kg, IM). After placing the rat in a stereotaxic instrument, heart rate, end-tidal CO_2, and body temperature were monitored throughout the surgery and subsequent tracer injections.

Anterograde tracer injections

For anterograde tracer injections, MI cortex was exposed and functional representations within MI were identified by using ICMS to evoke brief twitches of the whiskers or forepaw. Cathodal pulse trains (0.7-ms pulses at 250 Hz for 80 ms) were administered by glass micropipettes (0.3 to 1.8 MΩ) that contained hypertonic (3M) saline. After the pipette was lowered to a cortical depth of 1.7 mm, ICMS was started at currents of 100–150 μA to produce clear twitches in the forepaw or mystacial whisker pad. Between 4 and 8 sites were stimulated in MI cortex in each rat, and the ICMS current at each site was reduced until threshold levels (~50 μA or less) were reached that produced just-noticeable twitches. In the whisker region, only a few whiskers in one or two rows showed responses when threshold currents were employed. Consistent with previous reports (Hoffer et al., 2003; Brecht et al., 2004). ICMS indicated that the MI whisker region has a topographic organization in which row A is located medially and row E is located laterally. Tracer injections in the MI whisker region were placed at ICMS sites that evoked whisker twitches in the B, C, or D rows because this increased the likelihood of labeling the central part of the MI whisker region while avoiding tracer diffusion into surrounding cortical areas. To identify an appropriate injection site in the MI forepaw region, we initially identified ICMS sites that evoked whisker twitches and then moved the stimulation electrode progressively more laterally until we located a forepaw site known to be at least 500 μm lateral to the edge of the MI whisker region, which was usually determined by finding a site in which threshold ICMS currents evoked movements in both the whiskers and the forepaw. In some cases, the electrode was simply moved 500 μm lateral to the first site that evoked movements in the forepaw alone. We used these same procedures in another study to identify appropriate MI sites for retrograde tracer injections, and the results revealed significant functional differences in the patterns of corticocortical inputs to the whisker and forepaw regions in MI (Colechio and Alloway, 2009).

The anterograde tracer was injected at three depths ranging from 1.2 to 1.7 mm below the pia. Although several different tracers, including Alexa-Fluoro (AF) and biotinylated dextran amine (BDA), were injected into MI cortex as described in the companion papers (see Alloway et al., 2008, 2009), the analysis of MI projections to the brainstem was restricted to 16 rats that received injections of Fluoro-Ruby (FR) (Molecular Probes,

Eugene, OR). We focused on FR-labeled terminals because this tracer produced the greatest amount of terminal labeling in the brainstem, both in terms of density and the overall number of labeled terminals. In these cases, a Hamilton syringe (Reno, NV) was placed in a compatible holder (model 5000, Kopf Instruments, Tujunga, CA), and a volume of FR ranging from 100 to 150 nl was pressure-injected into MI. After surgery was completed, each rat that received an anterograde tracer injection was placed in its home cage for 7–12 days before it was sacrificed for histology.

Retrograde tracer injections

For retrograde tracer injections, the lateral part of the cerebellum was exposed to enable insertion of a tungsten electrode into the facial nucleus. The electrode was inserted at a 50° angle from the sagittal plane, approximately 11 mm caudal to bregma and 9–10 mm lateral to the midline. To locate facial motoneurons that project to the peripheral whiskers, we administered orthodromic stimulation in cathodal pulse trains (50 μA, 0.7 ms pulses at 250 Hz for 80 ms) to produce ipsilateral whisker twitches. In addition, two electrodes were inserted into the peripheral whisker pad and we administered antidromic stimulation (1.0 ms pulses, 350 μA) at 100 Hz to locate neurons that showed high-fidelity responses at a constant latency. After observing orthodromic, antidromic, or both types of responses, the electrode was removed from the facial nucleus, and a micropipette (50 μm tip) containing a 2% solution of Fluoro-Gold (FG) was inserted in its place, 6.0 – 6.5 mm below the surface of the cerebellum. During insertion, a negative retention current was applied to the FG pipette to prevent tracer leakage as the pipette was advanced into the facial nucleus. Subsequently, FG was administered iontophoretically with positive current pulses (4 μA, 7 seconds on/off) for 40 minutes. After surgery was completed, each rat that received a retrograde tracer injection was placed in its home cage for 12 days before it was sacrificed.

Histology

Each rat was deeply anesthetized with sodium pentobarbital (100 mg/kg, i.p.) and then transcardially perfused with physiological saline, 4% paraformaldehyde in 0.1 M phosphate buffer (PB; pH 6.9), and 4% paraformaldehyde with 10% sucrose. Brains were sectioned coronally at a thickness of 60 or 80 μm, and the most caudal sections were obtained at the level of the pyramidal decussation. Two series of sections processed for tracer labeling were alternated with one series processed for anatomical landmarks as indicated by thionin or cytochrome oxidase (Wong-Riley, 1979; Land and Simons, 1985). Sections processed for FR were serially mounted, dried overnight, and then defatted and dehydrated before being coverslipped with Cytoseal. A combined FITC/TRITC filter set (51004v2, Chroma Technology; Rockingham, VT) was used to visualize FR labeling; a UV filter (11000v2, Chroma Technology) was used to see FG-labeled neurons.

Reconstructions of the distribution of terminal labeling

Beaded varicosities appearing along labeled terminals in the brainstem were plotted with an AccuStage reconstruction system (St. Paul, MN) mounted on an Olympus light microscope (BH-2) equipped with a range of objectives. Plotting was done with a 10X eyepiece in combination with either a 10X or 20X objective. Axonal varicosities contain vesicles (Kincaid and Wilson, 1996) and are associated with synaptic markers such as synaptophysin (Voigt et al., 1993; Meng et al., 2004), which suggests that they represent en passant synapses. These putative synapses were plotted with respect to well-defined anatomical boundaries, and these reconstructions were superimposed onto photomicrographs of adjacent sections that had been processed for thionin or cytochrome oxidase. The photomicrographs were acquired by a Retiga EX CCD digital camera (Q-imaging, Toronto, Canada) mounted on the Olympus light microscope. With the aid of an atlas (Paxinos and Watson, 1986), the photomicrographs were used to draw additional outlines of nuclei and

other anatomical landmarks. Subsequently, the plotted varicosities in each brain region were counted and tallied across sections. These sums were used to calculate the relative proportions and mean density of the labeled varicosities in more than a dozen brainstem regions.

Peak density analysis using confocal microscopy

The density of terminal labeling was not uniform, but could vary substantially from one site to another within each target structure. In regions where the density of terminal labeling was sparse-to-moderate, the Accustage plotting system produced accurate reconstructions of the locations of all labeled varicosities. In regions where terminal labeling was very dense, however, each labeled varicosity could not be individually visualized and plotted using conventional light microscopy. Although all target regions, including the most densely-labeled sites, were carefully plotted so that the reconstructions depict proportional changes in labeling density, the number of plotted varicosities at the most densely-labeled sites is probably a fraction of the varicosities that are actually present. Therefore, to determine more accurately the maximum or peak density of labeled varicosities in the most strongly-connected regions, confocal images were acquired so that each labeled varicosity within the image could be counted.

Multiple confocal images were acquired from those brainstem sites that contained the densest labeling as indicated by our plotted reconstructions. Each image was obtained by a Leica confocal microscope (TCS SP2 AOBS, Leica Microsystems, Mannheim, Germany) equipped with a 543 nm laser for FR excitation (detection band set to 565–630 nm). All confocal images were obtained at a magnification of 120X (63X oil objective with a 1.9 optical zoom) and each image represented a standard square area (125 μm on each side) that served as a “counting box.” Multiple images were acquired from sites with the regions of densest labeling, and these images varied slightly in their orientation and exact position to increase the likelihood of obtaining an optimal image that contained the highest possible number of labeled varicosities within the counting box. For each confocal image, a series of focal planes extending 15 μm in depth along the Z-axis were collapsed into a single image. These images were stored as TIF files, and their brightness and contrast were adjusted to improve visualization of the labeled axons and their beaded varicosities.

Each image or counting box was then imported into a viewing program (Deneba Systems, Inc., Canvas X; Miami, FL), and a drawing tool was used to place a small green dot on each labeled varicosity. The varicosities were marked by persons who were unaware of the animal group and brain region from which the image was obtained. Axonal enlargements having twice the diameter of the axon were marked, but only if an axon emerged from both sides. As in a previous study that quantified the density of labeled projections from the cortex to the striatum (Reep et al., 2008), enlargements appearing at the end of an axon or at the crossover points of two axons were not marked. After each varicosity had been marked with a green dot, the number of dots was counted by the software program, and the density of the labeled varicosities in the counting box was calculated.

RESULTS

We reconstructed anterograde labeling in the brainstems of 26 rats used previously to characterize MI projections to the neostriatum, thalamus, and claustrum (Alloway et al., 2009). The brainstem reconstructions were obtained from sections that started at the commissure of the superior colliculus and continued caudally until the pyramidal decussation was reached. The nucleus cuneatus was present in the most caudal sections, but labeling in this structure was not reconstructed because a complete series of sections throughout its full extent was not always obtained. Labeled projections to the pons, superior

colliculus, and other brainstem regions were observed in every case, but brainstem labeling was reduced in cases in which only small amounts of tracer infiltrated the deep layers (Vb and VI) of MI. Furthermore, when compared to AF or BDA, the overall number and density of labeled terminals in the brainstem was noticeably higher when FR was injected into MI cortex. Regardless of the reasons for these tracer differences (e.g., transport efficiency, histologic processing, microscopic visualization), we restricted our analysis of brainstem labeling to 16 rats in which FR infiltrated the deepest layers of MI cortex and produced the maximal amount of brainstem labeling.

As shown in Table 1, we analyzed brainstem projections from 8 rats that received FR injections in the MI whisker region and from another 8 rats that received FR injections in the MI forepaw representation. Tracer injections were similar for both groups and usually produced dense deposits of labeling that occupied a column-like region no more than 600–800 μm in diameter. The mean FR injection volume for the MI whisker group was 130.8 ± 7.5 nl (mean ± SEM), whereas the mean volume for the MI forepaw group was 127.7 ± 6.3 nl ($t = 0.31$, $p > 0.05$).

As demonstrated by Figure 1, functional representations in MI cortex were consistent across rats. Microstimulation in the MI whisker cases revealed a clear topographic organization in which the A-row whiskers were most medial and the E-row whiskers were most lateral (Hoffer et al., 2003;Brecht et al., 2004). Most tracer injections in the MI whisker region were rostral and lateral to the rhythmic whisking area in which prolonged ICMS evokes repetitive whisker movements (Haiss and Schwarz, 2005). Because of tracer diffusion, however, some of the labeled projections in the MI whisker group may have originated from sites in the rostral part of the rhythmic area. The stereotaxic coordinates for the MI forepaw injections were at least 500 μm lateral to sites that evoked whisker twitches in the E-row, and this is consistent with the relative position of the forepaw-related tracer injections that are illustrated in Figure 1.

As illustrated by Figure 2, whisker-related and forepaw-related tracer injections were in separate parts of MI cortex. In cases where thionin staining was used to reveal the cytoarchitecture of MI cortex, the whisker-related injections were in medial agranular (Agm) cortex and the forepaw-related injections were in the lateral agranular (Agl) cortex. This finding was described in our previous reports (Alloway et al., 2008,2009), and it agrees with ICMS maps of the whisker and surrounding representations in cytoarchitectonically-defined regions in MI cortex (Brecht et al., 2004). Furthermore, the border between Agm and Agl is located slightly lateral to the apex of the external capsule, which is formed by the fibers of the cingulum. The proximity of the Agm-Agl border to the cingulum is depicted in many atlases (Paxinos and Watson, 1986), but the functional subdivisions on either side of the border have historically been labeled as frontal cortical area 1 (Agl) and frontal cortical area 2 (Agm). Therefore, as shown in Figure 2, the location of a tracer injection with respect to the cingulum provides an additional landmark for indicating whether the tracer was confined to the MI whisker or MI forepaw region. In the present study, tracer injections at ICMS sites that evoked whisker movements were medial to the cingulum, whereas tracer injections at sites that evoked forepaw movements were lateral to this landmark.

Further evidence for the functional confinement of the tracers in the whisker or forepaw regions comes from clear distinctions in the terminal labeling patterns of these two groups. We observed labeled terminals in the nucleus cuneatus when the MI forepaw region was injected but not when tracers were placed in the MI whisker region. Furthermore, as reported previously (Alloway et al., 2008, 2009), tracer injections in the MI whisker region produced dense terminal labeling in the contralateral thalamus and claustrum, but the

amount of contralateral labeling in these regions was practically nil when the MI forepaw region was injected.

Brainstem projections from the MI whisker region

Injections of FR into the MI whisker region revealed extensive labeling of axon terminals in specific brainstem regions. As illustrated by Figure 3, an injection in the MI whisker region (same experimental case shown in Figure 2D) produced dense labeling in parts of the superior colliculus (SC), the periaqueductal gray (PAG), the basal pons, and the deep mesencephalic (DpM) nucleus. Consistent with previous reports (Hattox et al., 2002), we also observed labeling in the interstitial nucleus of the medial longitudinal fasciculus (IMLF), the anterior pretectal (APT) nucleus, the red nucleus (RN), the dorsomedial tegmentum (DMT), and in several reticular nuclei including the pontine reticular nucleus (PnRt), the gigantocellular reticular nucleus (GiRt), the intermediate reticular nucleus (IRt), and the parvocellular reticular nucleus (PcRt). Reticular nuclei are often subdivided into different subregions (Paxinos and Watson, 1986), but the boundaries between these subregions were not distinct in our histological material. Hence, we did not try to distinguish between the oral and caudal subregions in PnRt or between the alpha, ventral, dorsal, and lateral subregions of GiRt. Furthermore, because we did not use any neurochemical markers to identify serotonergic neurons, some of the serotonergic regions that have been implicated with whisking behavior, such as the raphe obscurus (Hattox et al., 2003), were probably included in the area that we classified as GiRT.

Sections near the decussation of the superior cerebellar peduncle (xscp) usually contained a small number of labeled varicosities just dorsal to the medial lemniscus. Because of their close proximity to the medial lemniscus, we classified these varicosities as being in the B9 region (Paxinos and Watson, 1986). Sparser terminal labeling was observed less consistently in the oculomotor nucleus, the reticulotegmental nucleus (RtTg) and, even more rarely, in the inferior colliculus (IC) and medial geniculate nucleus (MGN). Low densities of FR-labeled terminals were occasionally observed in a few other areas, but these regions could not be identified with certainty because they were not associated with specific landmarks in the sections processed for CO or thionin. Collectively, these unidentified regions accounted for less than 2% of the brainstem varicosities that were plotted in our reconstructions and they were not included in our subsequent quantitative analysis.

As illustrated by Figures 3, 4, and 5, inspection of the reconstructions as well as microscopic examination of the tissue indicates that the densest brainstem labeling was in the SC, PAG, and basal pontine nuclei. Labeling in the SC, for example, extended rostrocaudally for at least 1.5 mm and most labeled varicosities were concentrated in the intermediate and deep layers. Although some labeled terminals appeared in the contralateral SC, the vast majority of corticotectal projections terminated ipsilaterally. Consistent with other studies that characterized corticotectal projections from Agm or the MI whisker region (Reep et al., 1987; Miyashita et al., 1994; Hattox et al., 2002), we consistently observed dense arbors of labeled terminals throughout much of the InG, InW, and DpG layers. This labeling pattern is represented in Figures 3 and 4 (see panels 3A, 3B, 4A``, 4B, 4C), which illustrate the dense laminar strips of SC labeling that appeared in many sections. Photomicrographs of the densest regions of SC labeling revealed dozens, perhaps hundreds, of labeled varicosities strung along the labeled axons that infiltrated these layers (Fig. 4B, 4C). In several sections, the densest labeling was concentrated in the intermediate (InG) and deep gray (DpG) layers with only a few labeled axons and varicosities in the intervening intermediate white (InW) layer.

Terminal labeling in the PAG appeared primarily on the ipsilateral side of this structure. As shown by the reconstructions in Figures 3 and 4, labeled projections from the MI whisker

region to PAG were concentrated in two regions. One region was located in the dorsal part of the PAG, whereas the other region was in the lateral part of the PAG near the SC and IMLF. Consistent with other studies (Reep et al., 1987; Hattox et al., 2002), labeling in these PAG regions was frequently characterized by tight clusters of overlapping axonal terminals that contained beaded varicosities at regular intervals (see Fig. 4D, 4E). Terminal labeling also appeared in other parts of the PAG, however, including regions located between the densest labeling. Landmarks distinguishing different PAG subregions were not clearly defined and, therefore, all of the labeled varicosities plotted in the PAG were summed together for our quantitative analyses.

As shown by Figure 5, even though the majority of terminal labeling in the basal pons was ipsilateral to the tracer injections in the MI whisker region, a sizeable fraction of the pontine labeling appeared on the contralateral side. The rostrocaudal extent of labeling in the basal pons was more limited than in the SC or PAG, partly because the basal pontine nuclei are not as extensive along this axis. Like other studies that characterized corticopontine projections from the whisker regions in sensorimotor cortex (Leergaard, 2003;Leergaard et al., 2004;Hoffer et al., 2005), we consistently observed several dense patches or clusters of labeled terminals that were concentrated in just a few sections in the rostral half of the pons. As seen in Figure 5 (panels B and C), the densest terminal labeling in the pons was characterized by hundreds of overlapping terminals in a small area. Indeed, the high concentration of terminal labeling in the basal pons prevented our reconstructions from duplicating the true density of the labeled varicosities in this structure.

We observed terminal labeling in numerous regions that comprise the reticular core of the brainstem. In addition to the DpM and DMT, several reticular nuclei contained labeled terminals, including the rostral and caudal PnRt, and the GiRt, IRt, and PcRt. Terminal labeling in the DpM, DMT, and PnRt was largely on the ipsilateral side, but labeling in the GiRT, IRt and PcRt was more evenly distributed across both sides of the brainstem. Although these regions usually contained dozens of labeled terminals and their varicosities, these axonal processes were widely scattered and never approached the density of labeling seen in the SC, PAG, or basal pons. Terminal labeling in most parts of the reticular nuclei consisted of one axonal arbor that contained a few collaterals and beaded varicosities; we rarely observed overlapping labeled axons in the PnRT, GiRt, IRt, or PcRt. There were some regional variations, however, that were consistently observed across different cases. Although GiRt labeling was generally sparse, the labeled axons and varicosities in this region were somewhat more concentrated in the alpha zone near the medial lemniscus and midline raphe, which is consistent with a previous study (Hattox et al., 2002). Finally, although we sometimes observed a few labeled terminals in the reticular nuclei around the facial nucleus, we never observed labeled axons entering any part of the facial nucleus.

Brainstem projections from the MI forepaw region

As indicated by Figure 6, injections of FR into the MI forepaw region (see Fig. 2B`) revealed widespread terminal labeling throughout many parts of the brainstem. The densest brainstem labeling in the MI forepaw cases was observed in the basal pontine nuclei (see Fig. 6D). Although some corticopontine projections from the MI forepaw region terminated on the contralateral side, the vast majority of the MI corticopontine projections innervated the ipsilateral side and many of these terminated more laterally than the corticopontine projections from the MI whisker region. Like the corticopontine projections from the MI whisker region, those from the MI forepaw region frequently produced several dense patches of labeled terminals that were separated by regions of less dense labeling. Furthermore, the high density of labeling in these patches prevented us from plotting the location of every labeled varicosity.

We also observed dense terminal labeling in the ipsilateral superior colliculus. As seen in Fig. 6A and 6B, the MI forepaw region projects mainly to the lateral part of the superior colliculus. Although the majority of SC labeling appeared in the InG and DpG layers, many labeled terminals and their varicosities were present in the intervening white layer.

Several differences in the distribution of projections from the MI forepaw and whisker regions were apparent in our reconstructions of plotted terminals. In general, the overall amount of brainstem labeling was greater in the MI whisker cases even though the size and volume of the tracer injections were similar in both groups. Among the 16 cases that we analyzed, the mean number of brainstem varicosities that we plotted in the MI whisker cases (5615 ± 1202) was more than 50% greater than the number of varicosities plotted in the MI forepaw cases (3553 ± 768). Second, we observed substantial labeling throughout widespread parts of the PAG in the MI whisker cases, but fewer labeled varicosities appeared in the PAG when the MI forepaw region was injected. Third, while we observed some labeling in the APT of the MI whisker cases, the APT labeling in the MI forepaw cases was noticeably denser. In fact, the APT nucleus was easily recognized in sections processed for CO, and we always observed dense labeling in the APT of the MI forepaw cases that was segregated from equally dense patches of labeling located nearby in the ventrolateral part of the SC (see Fig. 6A). Finally, in contrast to the MI whisker cases, the caudal levels of the MI forepaw cases contained substantial labeling in the pyramidal tract. Some of these labeled fibers diverged from the pyramidal tract to terminate in the nucleus cuneatus (see Fig. 5 in Alloway et al., 2009), whereas the rest continued caudally, presumably to innervate lower segments of the cervical spinal cord.

Brainstem projections from the MI whisker and forepaw regions displayed several similarities. In both groups of rats, projections to the central core regions of the brainstem, including several reticular nuclei, were similar in terms of density, lateralization, and overall distribution. Labeled projections to the rostral part of the DpM, for example, were moderately dense and terminated mainly on the ipsilateral side for both groups of rats. The density of labeling was comparatively sparse in all of the reticular nuclei, regardless of whether the tracer was injected into the whisker or forepaw regions of MI. For both groups of animals, however, reticular labeling was noticeably greater in the PnRt and GiRt than in the PcRt or IRt. Labeling in the PnRt was always densest on the ipsilateral side, and labeled projections to the GiRt were most likely to terminate in the ventral part of that structure. Terminal labeling was extremely sparse in the PcRt and IRt for both groups of animals. For animals that received tracer injections in the MI forepaw region, the IRt and PcRt were the only brainstem regions in which terminal labeling was more likely on the contralateral side. Variations in the amount of labeling in these nuclei were relatively high, however, and statistical analysis failed to detect any group differences in the lateralization of labeling in these reticular nuclei (see Fig. 7).

Quantitative analysis of brainstem projection patterns

After plotting the location of the labeled varicosities and superimposing these reconstructions onto the boundaries of structures in adjacent sections processed for CO or Nissl material, we counted the number of plotted varicosities in each of the outlined structures. The left part of Figure 7 depicts the distribution of plotted varicosities in the 13 brainstem regions that contained nearly all of the terminal labeling in the brainstems that we analyzed. Because the absolute number of plotted varicosities varied across cases, the regional distributions were expressed as a percentage of the total sum of varicosities that were plotted in each animal case.

As the left part of Figure 7 indicates, the majority of the MI projections to the brainstem appeared in two large structures known for their involvement in motor control. When the MI

forepaw region was injected, nearly 40% of the plotted varicosities appeared in the basal pons and another 25% appeared in the SC. Similarly, nearly 30% of the plotted varicosities in the MI whisker cases appeared in the SC, whereas another 24% appeared in the basal pons.

The remaining labeling was concentrated in just 3 or 4 regions for both groups of rats. Among rats that received tracer injections in the MI whisker region, the highest fraction of labeling after the SC and PN was in the DpM (12.5%), the PAG (11.9%), the PnRt (8.3%), and the GiRt (5.8%). Likewise, following tracer injections in the MI forepaw region, the highest fraction of labeling after the PN and SC was in the DpM (11.6%), the APT (8.4%), and the GiRt (3.8%). For both groups of rats, each of the remaining 6 or 7 brain regions contained less than 2% of the plotted varicosities that were analyzed.

Statistical analysis of the distributions in Figure 7 revealed several significant findings. An analysis of variance indicated that brain region was a significant factor in the distribution of labeled terminals ($F = 128.7$; $P < 0.0001$). Furthermore, a significant interaction existed between injection sites (MI whisker vs. MI forepaw) and the target brainstem regions ($F = 10.7$; $P < 0.0001$). A comparison of the two groups of animals revealed that the MI whisker injections produced proportionately more labeling in the PAG, PnRt, and DMT, whereas the MI forepaw injections produced proportionately more labeling in the basal pons and APT (Student t-test, $P < 0.01$ in each case).

As indicated by Figure 7(right), most of the MI projections to the brainstem terminated on the side ipsilateral to the injection site. With few exceptions, the ipsilateral side contained more than 75% of the labeled varicosities that were plotted in each brainstem region. The major exceptions include 3 reticular nuclei (ie., GiRt, PcRt, IRt) in which labeled varicosities were more evenly distributed across both sides of the brainstem. Consistent with these findings, the relative ratio of ipsilateral and contralateral labeling varied significantly across different brain regions ($F = 21.4$, $P < 0.0001$).

We detected a significant interaction between MI injection site and the regional ratio of ipsilateral and contralateral labeling ($F = 2.7$, $P < 0.01$), but only two brainstem regions showed significant shifts in this ratio as a function of MI injection site. Among these, the basal pons showed the largest shift between the two groups of rats. The ipsilateral PN received 92.8% of the labeled projections from the MI forepaw region but only 74.9% of those from the MI whisker region ($t = 5.66$, $P < 0.0001$). This distinction is notable because the output of the pontocerebellar system is transmitted rostrally to forebrain regions that ultimately project back to MI cortex (Groenegen and Witter, 2004; Ruigrok, 2004). Hence, MI whisker information processed by the pontocerebellar system is more likely to be transmitted to the MI whisker regions in both hemispheres.

Quantitative analysis of varicosity density

To assess the relative strength of MI projections to different brainstem regions, we measured the mean density of plotted varicosities in the regions identified in Figure 7. For this purpose, the smallest possible polygon was drawn around varicosities plotted in each region of each reconstructed section. The polygons consisted entirely of convex angles, and each vertex represented the location of a varicosity. When all polygons were drawn, the total number of plotted varicosities in the region was divided by the summed area of the polygons to yield mean density. For each region, this procedure was done only on the brainstem side that contained the most plotted varicosities (see Fig. 7, right).

Figure 8 illustrates the mean density of labeled varicosities that were plotted in the 13 brainstem regions that we analyzed. Mean density varied significantly as a function of

brainstem region ($F = 21.5$, $P < 0.0001$), but not as a function of MI injection site ($F = 0.13$, $P > 0.70$). Furthermore, we did not detect a significant interaction between MI injection site and brainstem region ($F = 2.04$, $P > 0.01$), and this indicates that the mean density of varicosities in most brainstem regions was similar for both groups of rats.

Based on the 26 data sets that we analyzed (13 brain regions x 2 MI injection sites), the basal pons contained the highest mean density of plotted varicosities. In addition, the APT, IMLF, PAG, and B9 region also had mean densities above the median, but these regions were relatively small and contained only a small fraction of the total labeling in the brainstem (see Fig. 7). None of these regions, however, are known for sending projections to the facial nucleus. Among brainstem regions that project to the facial nucleus (Hattox et al., 2002), the SC and RN had mean densities above the median but the DpM, GiRt, PcRt, and IRt had mean densities below the median. In fact, as shown in Fig. 8, when FR was injected into the MI whisker region, the mean density of plotted varicosities in the SC was more than 50% higher than in the DpM and 2–3 times higher than in the reticular nuclei (ie., PnRt, GiRt, PcRt, InRt).

While the mean density of plotted varicosities provides some measure of the relative strength of MI projections to different brainstem targets, this index can be misleading if the labeling density is not uniform throughout each target region. In the SC, for example, labeled varicosities were very dense in the gray layers but not in the intervening white layers. Furthermore, although our plotted reconstructions are fairly accurate when labeling density is sparse-to-moderate, conventional microscopy cannot reconstruct the location of all labeled varicosities when terminal labeling is very dense. In addition, focal brainstem sites in which terminal labeling is highly concentrated are much more likely to be activated by the injected regions in MI than locations in which the terminal labeling is below the mean density for that structure. For these reasons, we measured the peak or maximum density of labeled varicosities in the six brainstem regions (pons, SC, PAG, DpM, GiRt, and PnRt) that contained more than 85% of the varicosities that we plotted (see Figure 7, left). To determine the peak density in these six regions, we used confocal microscopy to obtain multiple images from the areas that contained the densest terminal labeling as indicated by our plotted reconstructions. This analysis was limited to the 3 rats in each group (MI whisker vs. MI forepaw) that contained the largest total number of plotted varicosities.

As seen in Figure 9, each confocal image was obtained at a magnification that represented a square area of 125 μm on each side. When viewed on a computer monitor, nearly all of the varicosities were clearly visualized and could be marked for our density measurements. When images from the basal pons and SC were inspected, however, some sites contained overlapping terminals that precluded visualization of each individual varicosity. Nonetheless, we counted all rounded enlargements that could be discerned in which a thin axon departed from opposite sides of the enlargement. In most cases, these varicosities appeared as a series of enlargements like beads on a string. We did not count enlargements that appeared at the terminal ends of axons, as these may represent the end of a cut axon. We also did not count small bright spots where two axons crossed each other. Similar criteria were used previously to measure the density of corticostriatal projections from MI cortex (Reep et al., 2008).

The peak densities for the six brain regions that contained the largest number of labeled terminals are illustrated in Figure 10. In this figure, regional differences in peak density are depicted as absolute and normalized values in panels A and B, respectively. An analysis of variance indicates that brain region had a significant effect on peak labeling density regardless of whether we analyzed absolute or normalized values ($F > 23.0$; $P < 0.0001$ in both cases). In each rat that we analyzed, peak density was always highest in the basal pons.

Among the whisker cases that we analyzed, the second highest peak density was in the SC, and this density was nearly 4 times higher than the peak density in the PnRt and at least 5–6 times higher than the peak density in the GiRt.

Retrogradely-labeled projections to the facial nucleus

Injections of anterograde tracers into MI cortex did not reveal any labeled terminals in the facial nucleus. However, if only one part of MI cortex projects directly to the facial nucleus, our tracer injections may have missed this critical region. To rule out this possibility, we injected the facial nucleus with a retrograde tracer to determine if this experimental approach might produce neuronal labeling in specific parts of MI cortex.

We injected FG into the facial nucleus of 3 rats. In each case, we used orthodromic and/or antidromic electrical stimulation to locate the sites in the facial nucleus that contained whisker-related motoneurons. Our injections into these sites produced dense concentrations of FG in the lateral facial nucleus, and this is consistent with previous studies showing that this subnucleus represents the origin of efferent projections to the whisker pad (Klein and Rhoades, 1985; Semba and Egger, 1986; Herfst and Brecht, 2008). As shown by one example in Figure 11, the tracer infiltrated most of the lateral facial nucleus and diffused into surrounding parts of the intermediate facial nucleus.

Tracer injections into the lateral facial nucleus produced neuronal labeling in several brainstem regions. As illustrated by Figure 12, hundreds of brightly-lit FG-labeled neurons were distributed throughout the midbrain, especially on the side contralateral to the injection site. Consistent with other reports (Miyashita and Mori, 1995; Hattox et al., 2002), we observed dense neuronal labeling in the contralateral RN, the ventromedial PAG near the oculomotor nucleus, and in the ipsilateral Kolliker-Fuse nucleus. The deep gray layer of the SC also contained dense neuronal labeling that was narrowly separated from clusters of labeled neurons in the more ventral-lying DpM (see Fig. 12 C,D,E). We also observed labeled neurons in many parts of the reticular nuclei, especially in the PnRt and more caudally near the facial nucleus. The ventral parts of the GiRt, IRt, and PcRt nuclei that were closest to the facial nucleus contained several patches of brightly-lit neurons.

Inspection of MI cortex revealed some FG-labeled neurons in the hemisphere contralateral to the FG injection site. Compared to the brainstem, however, the number of labeled neurons in MI was extremely low. The largest number of labeled MI neurons in the three cases was only 25 cells, and the FG injection shown in Figure 11 produced only 14 labeled neurons in MI. The vast majority of labeled neurons in MI appeared in coronal sections located rostral to the caudate-putamen. This region, which is approximately 2.7 to 3.3 mm rostral to bregma, is more rostral than all of our FR injections in MI (see Fig 1). As indicated by Figure 13, many labeled neurons in MI were clustered in the transitional region between Agm and Agl. The second most likely MI region to contain labeled neurons was located more laterally, usually 2.2 to 3.0 mm lateral to the midline. Based on previous mapping studies in MI, this far lateral region of Agl probably contains the jaw, lip, and tongue representations (Hall and Lindholm, 1974; Neafsy and Sievert, 1982). Given that the intermediate facial nucleus innervates muscles of the jaw and lip (Hinrichsen and Watson, 1984), FG-labeled neurons in the most lateral parts of MI could be due to the spread of our FG injections into the intermediate facial nucleus.

DISCUSSION

This study characterized the relative strength of MI projections to several brainstem regions in the rat. Among the main findings, the whisker and forepaw regions in MI project more strongly to the basal pons than to any other brainstem region. Although the total number of

plotted varicosities in the SC and basal pons were similar, differences in the size of the innervated areas meant that the mean density of labeling was substantially higher in the pons than in the SC. In addition, regardless of whether we measured the mean or peak density of labeled varicosities, both measurements indicate that MI projections to the pons and the SC are considerably stronger than the projections to the reticular formation. This is in contrast to a previous study which reported that MI projects equally strongly to the SC and GiRt (Hattox et al., 2002).

Furthermore, whereas the vast majority of corticopontine projections from the MI forepaw region terminate ipsilaterally, a large fraction of the projections from the MI whisker region terminate on the contralateral side of the basal pons. This finding is significant because the output of the pontocerebellar system is sent to the forebrain, where many interhemispheric connections are present for coordinating the bilateral movements of the whiskers (Alloway et al., 2009).

Following anterograde tracer injections into MI, we did not observe any labeled terminals in the facial nucleus. Consistent with this finding, retrograde tracer injections into the lateral facial nucleus produced very few labeled neurons in MI. By comparison, we observed hundreds of retrogradely-labeled neurons in SC, DpM, RN, and other brainstem regions that are known for their projections to the facial nucleus. Together, our anterograde and retrograde tracing results suggest that the SC provides the most effective route for transmitting information from the MI whisker region to the facial nucleus.

Technical considerations

Reconstructing the patterns of labeled terminals and their putative synaptic contacts poses several challenges in determining which postsynaptic targets of MI cortex receive the strongest functional projections. One problem concerns the difficulty of identifying and plotting every labeled varicosity when labeling density is high. As in previous studies (Hoffer et al., 2005; Alloway et al., 2009), the topographical reconstructions resembled the labeling patterns that we visualized through the microscope. Using this guideline, the number and density of plotted varicosities in the reconstructions should be proportional to the actual number and density of varicosities in the tissue. Nonetheless, while our reconstructions probably depict almost all of the labeled varicosities in sparsely- or moderately-labeled regions, the number of varicosities plotted in densely-labeled regions probably represents a fraction of the actual number of labeled varicosities in those regions. To determine the density of synaptic contacts in the most densely-labeled regions, we subsequently used confocal microscopy to obtain high resolution images so that we could mark each labeled varicosity and count the number of putative synapses in a standardized area. Although this procedure cannot be performed throughout the entire brainstem, this technique effectively measured the maximum density of labeled varicosities in the six brain regions (pons, SC, PAG, DpM, PnRt, GiRt) that contained the most labeled terminals. While the mean density of plotted varicosities provides one approach for rank-ordering the relative strength of MI projections to different brainstem regions, the peak or maximum density of labeled varicosities provides another method for assessingwhich brainstem targets are most likely to be activated by inputs from MI.

A potential interpretative problem concerns the fact that the density of synaptic contacts is not the only factor that determines the efficacy of neurotransmission between a pair of brain regions. The likelihood that a postsynaptic target will respond to excitatory inputs from MI or any other brain region depends on several factors, including the dendritic locations of the synaptic inputs, their proximity to the soma and axon hillock, their relative input timing, and the biophysical properties of the postsynaptic neuron. Serial interactions between brain regions are also influenced by other “third-party” brain regions that may gate the effects of a

region on its postsynaptic target. Nonetheless, to the extent that the density of synaptic inputs is related to the efficacy of neurotransmission, our results indicate that MI inputs should have a stronger impact on the SC and basal pons than on other brainstem regions. Hence, our data provide a strong rationale for using electrophysiology techniques (e.g. cross-correlation analysis) to test the prediction that the MI whisker region is more strongly connected with the pons and SC than with other brainstem regions.

Corticopontine projections from MI

The present study indicates that both the whisker and forepaw regions in MI send dense projections to the basal pontine nuclei. This finding is consistent with a large body of data showing that MI, SI, and related sensorimotor regions provide the bulk of the cortical projections to the basal pons (Wiesendanger and Wiesendanger, 1982; Legg et al., 1989;Ruigrok, 2004). We also found that MI projections terminate more densely in the basal pons than in the SC or any other brainstem regions. Similarly, we previously reported that projections from SI barrel cortex provide denser inputs to the basal pons than to the SC (Hoffer et al., 2005). Hence, even though many corticotectal and corticopontine projections from sensorimotor cortex represent collaterals of the same neuron (Hallman et al., 1988; Glickstein, 2003), the axonal arbors that innervate the pons consistently display denser patterns of synaptic contacts. Presumably, these dense contacts should produce a corresponding increase in the efficacy of neurotransmission in the corticopontine pathway.

Information transmitted by the corticopontine pathway is relayed to the cerebellum, which sends its output to many brain regions including the RN, the SC, extensive parts of the reticular formation, and motor-related nuclei in the thalamus (Ruigrok, 2004). The thalamic regions, which include the ventrolateral and ventromedial nuclei, send the bulk of their projections to sensorimotor cortical areas that include MI (Groenegen and Witter, 2004). Hence, to some extent, MI corticopontine projections represent the initial part of a multisynaptic loop that eventually terminates back in MI and other sensorimotor cortical areas.

This is significant when considered with respect to differences in the relative proportion of ipsilateral and contralateral projections that originate from the whisker and forepaw regions of MI. While 93% of the corticopontine projections from the MI forepaw region terminate in the ipsilateral pons, this proportion decreases to 74% for corticopontine projections from the MI whisker region. In almost all other brainstem regions that received projections from MI, the relative proportions of ipsilateral and contralateral projections were similar for both groups of injections (compare MI forepaw and MI whisker groups in Fig. 7). Conversely, in our previous studies of MI projections to the forebrain (ie., thalamus, neostriatum, claustrum), which included many of the same cases described in the present report, we consistently observed more interhemispheric (ie., contralateral) projections from the MI whisker region than from the MI forepaw region (Alloway et al., 2008,2009). The greater proportion of contralateral projections from the MI whisker region is consistent with our hypothesis that interhemispheric connections in the forebrain represent a major part of the neural substrate for coordinating whisker movements bilaterally. Given that the pontocerebellar system sends its output to the forebrain, the increased proportion of MI whisker projections to the contralateral pons supports the view that these projections have a role in coordinating bilateral whisker movements.

Corticotectal projections from MI

Consistent with previous reports (Reep et al., 1987; Miyashita et al., 1994; Hattox et al., 2002), the MI whisker regions send dense projections to the intermediate and deep layers of the SC. With the exception of the basal pons, our analysis indicates that the MI whisker

projections to the SC are more numerous and denser than to other brainstem regions. This is significant because, unlike the basal pons, the SC projects to the lateral facial nucleus (Miyashita et al., 1994; Miyashita and Mori, 1995; Hattox et al., 2002). Furthermore, when compared to other brainstem regions that project to the lateral facial nucleus, the density of MI synaptic contacts in the SC are several times greater than the density of MI synaptic contacts in the reticular nuclei (ie., PnRt, GiRt, PcRt, IRt).

Consistent with SC projections to the lateral facial nucleus, microstimulation of the SC evokes whisker movements (McHaffie and Stein, 1982; Hemelt and Keller, 2008). In contrast to the effects of prolonged MI stimulation, which evokes rhythmic whisking (Haiss and Schwarz, 2005; Cramer and Keller, 2006), prolonged stimulation of the SC evokes sustained protractions (Hemelt and Keller, 2008). No study, however, has recorded neuronal activity in the SC while administering MI stimulation that evokes rhythmic whisker movements. Furthermore, no study has characterized the relative timing and efficacy of neuronal interactions between MI and the SC during rhythmic whisking. In view of our data, which indicate a high density of MI projections to the SC, we predict that MI exerts a powerful influence on SC and that neuronal responses in the SC might display rhythmic responses to MI inputs during rhythmic whisking.

Corticoreticular projections from MI

Previous work had suggested that the MI whisker region has strong connections with several reticular nuclei (Hattox et al., 2002). Our analysis, however, indicates that GiRt and other reticular regions receive relatively sparse projections from the MI whisker region. In fact, the density of MI projections to the reticular nuclei (ie., GiRt, PcRt, IRt, PnRt) are dwarfed by the high density of MI projections to the SC. We obtained essentially the same results when we analyzed the labeled projections from the MI forepaw region. In fact, our results more closely resemble the findings of investigators who reported dense projections from Agm to the SC, PAG, and basal pons, but observed “no other brainstem labeling” (Reep et al., 1987).

Despite the relative paucity of MI projections to GiRt and related regions, several findings indicate that serotonergic neurons in the vicinity of GiRt, especially in the raphe obscurus and raphe magnus, play an important role in regulating the oscillations of whisker movements (Hattox et al., 2003; Cramer and Keller, 2006; Cramer et al., 2007). Whereas serotonergic agonists evoke rhythmic discharges from neurons in the lateral facial nucleus, serotonergic antagonists suppress this rhythmic activity. Furthermore, rhythmic whisker movements evoked by MI stimulation are associated with concomitant rhythmic activity in putative serotonergic neurons in the lateral part of the paragigantocellular nucleus.

To reconcile the relative lack of MI projections to the GiRt with data indicating the importance of serotonin in whisking behavior, we suggest that the SC should be considered as an alternate route for activating serotonergic circuits in the GiRt region. The SC and contiguous regions in the mesencephalic reticular formation project to several brainstem regions including PnRt, GiRt, and the raphe magnus (Redgrave et al., 1987; Shehab et al., 1995). In contrast to its ipsilateral projections, the contralateral projections from SC terminate in the GiRt and nearby regions along the midline (see Figures 5 and 6 in Redgrave et al., 1987). Hence, MI activation of serotonergic neurons along the midline and in other regions close to the GiRt could be achieved, in large part, by activating the SC and its efferent projections to contralateral reticular nuclei that project to the lateral facial nucleus. In this context, it is worth noting that microstimulation of the medullary serotonergic region evokes whisker protractions (Hattox et al., 2003). Microstimulation in the SC also evokes whisker protractions, although the SC-induced movements often persist beyond the application of the ICMS (Hemelt and Keller, 2008). Therefore, whisker movements evoked

by SC stimulation are probably mediated, at least in part, by downstream actions on serotonergic regions in the pontomedullary reticular formation. Presumably, the rhythmic whisking produced by MI microstimulation is correlated with temporal patterns of SC activity that differ from the temporal patterns produced by direct stimulation of the SC. In view of SC projections to the pontomedullary reticular formation (Redgrave et al., 1987; Shehab et al., 1995), our findings suggest that strong projections from MI to SC, coupled with weaker MI projections to other brainstem regions, activate a complex network of brainstem regions that regulate whisking behavior.

Acknowledgments

The authors thank Michelle Olson for helping with some of the tracer injections and for plotting some of the anterograde labeling that was visualized with conventional fluorescent microscopy. We also thank both Jon Harrold and Elizabeth Colechio for marking labeled varicosities in the confocal images.

Grant sponsor: NIH grants NS37532 and NS052689

LITERATURE CITED

Alloway KD, Olson ML, Smith JB. Contralateral corticothalamic projections from MI whisker cortex: Potential route for modulating hemispheric interactions. J Comp Neurol. 2008; 510:100–116. [PubMed: 18615539]

Alloway KD, Smith JB, Beauchemin KJ. Bilateral projections from rat MI whisker cortex to the neostriatum, thalamus, and claustrum: Forebrain circuits for modulating whisking behavior. J Comp Neurol. 2009; 515:548–564. [PubMed: 19479997]

Berg RW, Kleinfeld D. Vibrissa movement elicited by rhythmic electrical microstimulation to motor cortex in the aroused rat mimics exploratory whisking. J Neurophysiol. 2003; 90:2950–2963. [PubMed: 12904336]

Brecht M, Krauss A, Muhammad S, Sinai-Esfahani L, Bellanca S, Margie TW. Organization of rat vibrissa motor cortex and adjacent areas according to cytoarchitectonics, micro-stimulation, and intracellular stimulation of identified cells. J Comp Neurol. 2004a; 479:360–373. [PubMed: 15514982]

Colechio EM, Alloway KD. Differential topography of the bilateral cortical projections to the whisker and forepaw regions in rat motor cortex. Brain Struct Funct. 2009; 213:423–439. [PubMed: 19672624]

Cramer NP, Keller A. Cortical control of a whisking central pattern generator. J Neurophysiol. 2006; 96:209–217. [PubMed: 16641387]

Cramer NP, Li Y, Keller A. The whisking rhythm generator: a novel mammalian network for the generation of movement. J Neurophysiol. 2007; 97:2148–2158. [PubMed: 17202239]

Donoghue JP, Parham C. Afferent connections of the lateral agranular field of the rat motor cortex. J Comp Neurol. 1983; 217:390–404. [PubMed: 6886060]

Donoghue JP, Wise SP. The motor cortex of the rat: cytoarchitecture and microstimulation mapping. J Comp Neurol. 1982; 212:76–88. [PubMed: 6294151]

Gao P, Bermejo R, Zeigler HP. Whisker deafferentation and rodent whisking patterns: behavioral evidence for a central pattern generator. J Neurosci. 2001; 21:5374–5380. [PubMed: 11438614]

Gao P, Hattox AM, Jones LM, Keller A, Ziegler HP. Whisker motor cortex ablation and whisker movement patterns. Somatosen Mot Res. 2003; 20:191–198.

Gioanni Y, Lamarche M. A reappraisal of rat motor cortex organization by intracortical microstimulation. Brain Res. 1985; 344:49–61. [PubMed: 4041868]

Glickstein M. Subcortical projections of the parietal lobes. Adv Neurol. 2003; 93:43–55. [PubMed: 12894400]

Grinevich V, Brecht M, Osten P. Monosynaptic pathway from rat vibrissa motor cortex to facial motor neurons revealed by lentivirus-based axonal tracing. J Neurosci. 2005; 25:8250–8258. [PubMed: 16148232]

Groenegen, HJ.; Witter, MP. Thalamus. In: Paxinos, G., editor. The rat nervous system. New York: Academic Press, Inc.; 2004. p. 407-453.

Haiss F, Schwarz C. Spatial segregation of different modes of movement control in the whisker representation of rat primary motor cortex. J Neurosci. 2005; 25:1579–1587. [PubMed: 15703412]

Hall RD, Lindholm EP. Organization of motor and somatosensory neocortex in the albino rat. Brain Res. 1974; 66:23–38.

Hallman LE, Schofield BR, Lin CS. Dendritic morphology and axon collaterals of corticotectal, corticopontine, and callosal neurons in layer V of primary visual cortex of the hooded rat. J Comp Neurol. 1988; 272:149–160. [PubMed: 3385021]

Hattox AM, Li Y, Keller A. Serotonin regulates rhythmic whisking. Neuron. 2003; 39:343–352. [PubMed: 12873389]

Hattox AM, Priest CA, Keller A. Functional circuitry involved in the regulation of whisker movements. J Comp Neurol. 2002; 442:266–276. [PubMed: 11774341]

Hemelt ME, Keller A. Superior colliculus control of vibrissa movements. J Neurophysiol. 2008; 100:1245–1254. [PubMed: 18562549]

Herfst LJ, Brecht M. Whisker movements evoked by stimulation of single motor neurons in the facial nucleus of the rat. J Neurophysiol. 2008; 99:2821–2832. [PubMed: 18353915]

Hill DN, Bermejo R, Zeigler HP, Kleinfeld D. Biomechanics of the vibrissa motor plant in rat: Rhythmic whisking consists of triphasic neuromuscular activity. J Neurosci. 2008; 28:3438–3455. [PubMed: 18367610]

Hinrichsen CFL, Watson CD. The facial nucleus of the rat: Representation of facial muscles revealed by retrograde transport of horseradish peroxidase. Anat Rec. 1984; 209:407–415. [PubMed: 6465545]

Hoffer ZS, Arantes H, Roth R, Alloway KD. Functional circuits mediating sensorimotor integration: Quantitative comparisons of projections from rodent barrel cortex to MI cortex, neostriatum, superior colliculus, and pons. J Comp Neurol. 2005; 488:82–100. [PubMed: 15912501]

Hoffer ZS, Hoover JE, Alloway KD. Sensorimotor corticocortical projections from rat barrel cortex have an anisotropic organization that facilitates integration of inputs from whiskers in the same row. J Comp Neurol. 2003; 466:525–544. [PubMed: 14566947]

Kincaid AE, Wilson CJ. Corticostriatal innervation of the patch and matrix in the rat neostriatum. J Comp Neurol. 1996; 374:578–592. [PubMed: 8910736]

Klein BG, Rhoades RW. Representation of whisker follicle intrinsic musculature in the facial motor nucleus of the rat. J Comp Neurol. 1985; 232:55–69. [PubMed: 3973083]

Land PW, Simons DJ. Cytochrome oxidase staining in the rat SmI barrel cortex. J Comp Neurol. 1985; 238:225–235. [PubMed: 2413086]

Leergaard TB. Clustered and laminar topographic patterns in rat cerebro-pontine pathways. Anat Embryol. 2003; 206:149–162. [PubMed: 12592566]

Leergaard TB, Alloway KD, Pham TA, Bolstead I, Hoffer Z, Pettersen C, Bjaalie JG. Three dimensional topography of corticopontine projections from rat sensorimotor cortex: comparisons with corticostriatal projections reveal diverse integrative organization. J Comp Neurol. 2004; 478:306–322. [PubMed: 15368533]

Legg CR, Mercier B, Glickstein M. Corticopontine projection in the rat: the distribution of labelled cortical cells after large injections of horseradish peroxidase in the pontine nuclei. J Comp Neurol. 1989; 286:427–441. [PubMed: 2778100]

McHaffie JG, Stein BE. Eye movements evoked by electrical stimulation in the superior colliculus of rats and hamsters. Brai Res. 1982; 247:243–253.

Meng Z, Li Q, Martin JH. The transition from development to motor control function in the corticospinal system. J Neurosci. 2004; 24:605–614. [PubMed: 14736845]

Mitchinson B, Martin CJ, Grant RA, Prescott TJ. Feedback control in active sensing: Rat exploratory whisking is modulated by environmental contact. Proc Roy Soc B. 2007; 274:1035–1041.

Miyashita E, Keller A, Asanuma H. Input-output organization of the rat vibrissal motor cortex. Exp Brain Res. 1994; 99:223–232. [PubMed: 7523173]

Miyashita E, Mori S. The superior colliculus relays signals descending from the vibrissal motor cortex to the facial nerve nucleus in the rat. Neurosci Lett. 1995; 195:69–71. [PubMed: 7478258]

Molinari M, Minciacchi D, Bentivoglio M, Macchi G. Efferent fibers from the motor cortex terminate bilaterally in the thalamus of rats and cats. Exp Brain Res. 1985; 57:305–312. [PubMed: 3972032]

Neafsey EJ, Bold EL, Haas G, Hurley-Gius KM, Quirk G, Sievert CF, Terreberry RR. The organization of the rat motor cortex: a microstimulation mapping study. Brain Res. 1986; 396:77–96. [PubMed: 3708387]

Paxinos, G.; Watson, C. The Rat Brain in Stereotaxic Coordinates. second edition. New York: Academic Press; 1986.

Porter LL, White EL. Afferent and efferent pathways of the vibrissal region of primary motor cortex in the mouse. J Comp Neurol. 1983; 214:279–289. [PubMed: 6853758]

Porter LL, White EL. Termination of callosal afferents onto identified callosal projection neurons in the primary motor cortex of the mouse. Neurosci Lett. 1984; 47:37–40. [PubMed: 6087219]

Redgrave P, Mitchell IJ, Dean P. Descending projections from the superior colliculus in rat: a study using orthograde transport of whaetgerm-agglutinin conjugated horseradish peroxidase. Exp Brain Res. 1987; 68:147–167. [PubMed: 2826204]

Reep RL, Corwin JV, Hashimoto A, Watson RT. Efferent connections of the rostral portion of medial agranular cortex in rats. Brain Res Bull. 1987; 19:203–221. [PubMed: 2822206]

Reep RL, Wu JH, Cheatwood JL, Corwin JV, Kartje GL, Mir A. Quantification of synaptic density in corticostriatal projections from rat medial agranular cortex. Brain Res. 2008; 1233:27–34. [PubMed: 18691563]

Reiner A, Jiao Y, Del Mar N, Laverghetta AV, Lei WL. Differential morphology of pyramidal tract-type and intratelencephalically projecting-type corticostriatal neurons and their intra striatal terminals in rats. J Comp Neurol. 2003; 457:420–440. [PubMed: 12561080]

Rice, FL. Comparative aspects of barrel structure and development. In: Jones, EG.; Diamond, IT., editors. Cerebral Cortex. Vol. 11. The barrel cortex of rodents. New York: Plenum Press; 1995. p. 1-75.

Rouiller EM, Moret V, Liang F, Wiesendanger M. Patterns of corticothalamic terminations following injection of Phaseolus vulgaris leucoagglutinin (PHA-L) in the sensorimotor cortex of the rat. Neurosci Lett. 1991; 125:93–97. [PubMed: 1713320]

Ruigrok, TJH. Precerebellar nuclei and red nucleus. In: Paxinos, G., editor. The rat nervous system. New York: Academic Press, Inc.; 2004. p. 167-204.

Sachdev RN, Berg RW, Champney G, Kleinfeld D, Ebner FF. Unilateral vibrissa contact: changes in amplitude but not timing of rhythmic whisking. Somatoses Mot Res. 2003; 20:163–169.

Sellien H, Eshenroder DS, Ebner FF. Comparison of bilateral whisker movement in freely exploring and head-fixed adult rats. Somatosens Mot Res. 2005; 22:97–114. [PubMed: 16338819]

Semba K, Egger MD. The facial “motor” nerve of the rat: control of vibrissal movement and examination of motor and sensory components. J Comp Neurol. 1986; 247:144–158. [PubMed: 3722437]

Shehab S, Dean P, Redgrave P. The dorsal midbrain anticonvulsant zone – II. Efferent connections revealed by the anterograde transport of whaetgerm agglutinin-horseradish peroxidase from injections centred on the intercollicular area in the rat. Neuroscience. 1995; 65:681–695. [PubMed: 7541903]

Towal RB, Hartmann MJ. Right-left asymmetries in the whisking behavior of rats anticipate head movements. J Neurosci. 2006; 26:8838–8846. [PubMed: 16928873]

Veinante P, Dechenes M. 2003; 464:98–103.

Voigt T, De Lima AD, Beckmann M. Synaptophysin immunohistochemiostry reveals inside-out pattern of early synaptogenesis in ferret cerebral cortex. J Comp Neurol. 1993; 330:48–64. [PubMed: 8468403]

Welker WI. Analysis of sniffing in the albino rat. Behaviour. 1964; 12:223–244.

Wiesendanger R, Weisendanger M. The corticopontine system in the rat. II. The projection pattern. J Comp Neurol. 1982; 208:227–238. [PubMed: 7119159]

Wilson CJ. Postsynaptic potentials evoked in spiny neostriatal projection neurons by stimulation of ipsilateral and contralateral neocortex. Brain Res. 1986; 367:201–213. [PubMed: 3008920]

Wilson CJ. Morphology and synaptic connections of crossed corticostriatal neurons in the rat. J Comp Neurol. 1987; 263:567–580. [PubMed: 2822779]

Wong-Riley M. Changes in the visual system of monocularly sutured or enucleated cats demonstrable with cytochrome oxidase histochemistry. Brain Res. 1979; 171:11–28. [PubMed: 223730]

Abbreviations

3	oculomotor nucleus
6	abducens nucleus
7	facial nucleus
7n	facial nerve
8n	vestibulocochlear nerve
AF	Alexa-fluoro
Agl	agranular cortex, lateral
Agm	agranular cortex, medial
APT	anterior pretectal nucleus
B9	B9 region, hydroxytrptamine cells
BDA	biotinylated dextran amine
CO	cytochrome oxidase
cp	cerebral peduncle
DMT	dorsomedial tegmentum
DpG	deep gray layer, superior colliculus
DpM	deep mesencephalic nucleus
DpW	deep white layer, superior colliculus
DTg	dorsal tegmental nucleus
FR	Fluoro-ruby
GiRt	gigantocellular reticular nucleus
IC	inferior colliculus
ICMS	intracranial microstimulation
IMLF	interstitial nucleus of MLF
InG	intermediate gray layer
InW	intermediate white layer
IPA	interpeduncular nucleus, apical part
IPR	interpeduncular nucleus, rostral part
IRt	intermediate reticular nucleus
lfp	longitudinal fasciculus pons
LVN	lateral vestibular nucleus

mcp	middle cerebellar peduncle
MGN	medial geniculate nucleus
MI	motor cortex
ml	medial lemniscus
Mo5	motor trigeminal nucleus
MPB	medial parabrachial nucleus
MVN	medial vestibular nucleus
NLL	nucleus of lateral lemniscus
PAG	Periaqueductal Gray
PcRt	parvocellular reticular nucleus
PN	pontine nuclei
PnRt	pontine reticular nucleus
POm	posterior nucleus, medial
Pr5	principal trigeminal nucleus
py	pyramidal tract
RN	red nucleus
rs	rubrospinal tract
RtTg	reticulotegmental nucleus
s5	sensory root, trigeminal
SC	superior colliculus
scp	superior cerebellar peduncle
SNR	substantia nigra, pars reticulata
SO	superior olive
Sp5	spinal trigeminal nucleus
sp5	spinal trigeminal tract
SuG	superior gray layer, superior colliculus
tfp	transverse fibers of the pons
tz	trapezoid body
xscp	decussation, superior cerebellar peduncle

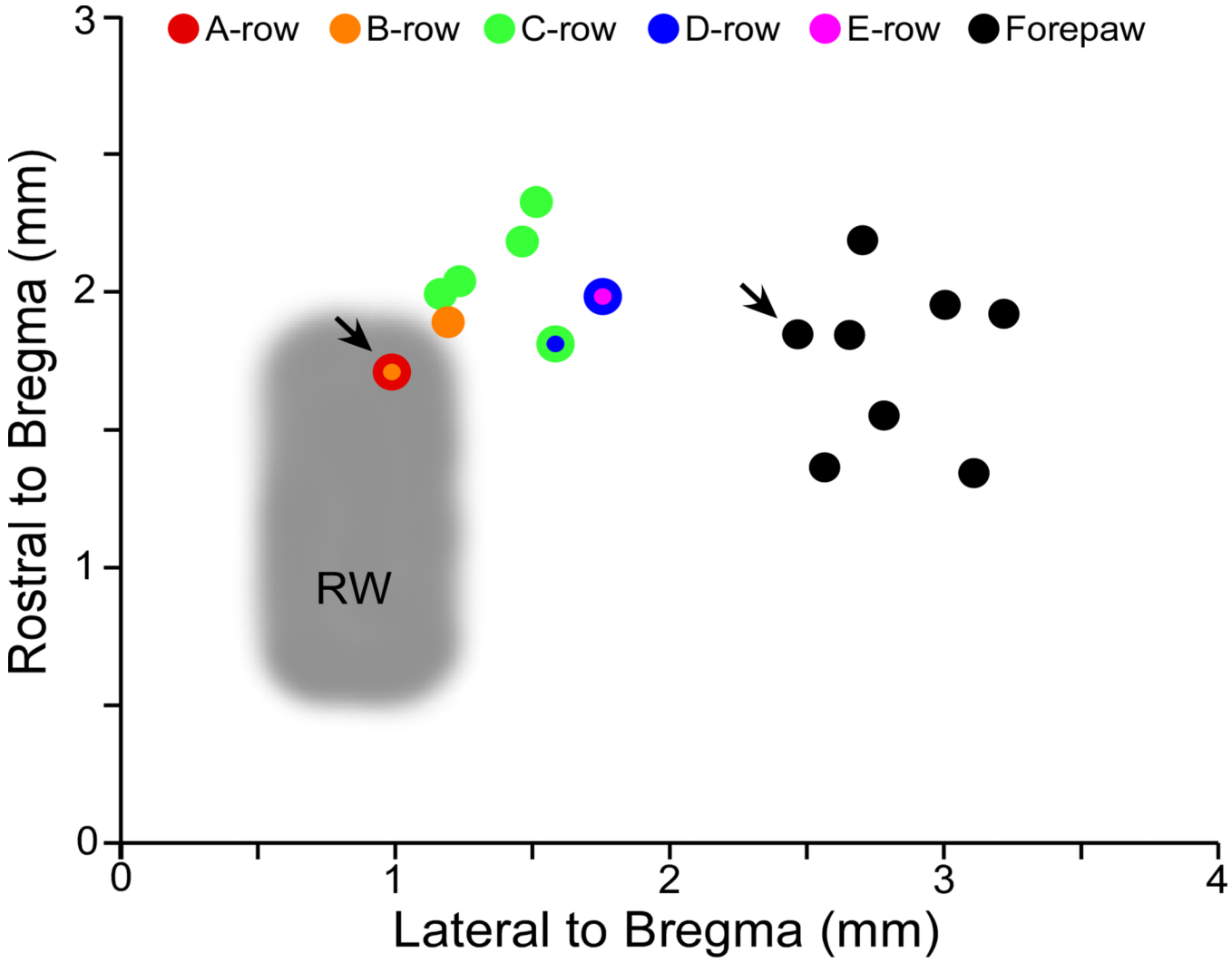

Fig. 1.

Distribution of Fluoro-ruby (FR) injection sites in primary motor (MI) cortex according to stereotaxic coordinates and the responses to intracranial microstimulation (ICMS). Sites where ICMS evoked movements of the contralateral forepaw are indicated by black circles. Sites that evoked whisker movements in a specific row are color-coded according to the legend; sites that evoked whisker movements in two rows are indicated by two colors. To compare the relative topography of injections across all 16 cases, FR injections in the left hemisphere (n = 2) are represented by mirror image coordinates for the right hemisphere. The two arrows indicate the FR injections for cases BN51 and BN53, results from which are illustrated in Figures 2 through 6. The gray region indicates the rhythmic whisking (RW) area identified by Haiss and Schwarz (2005).

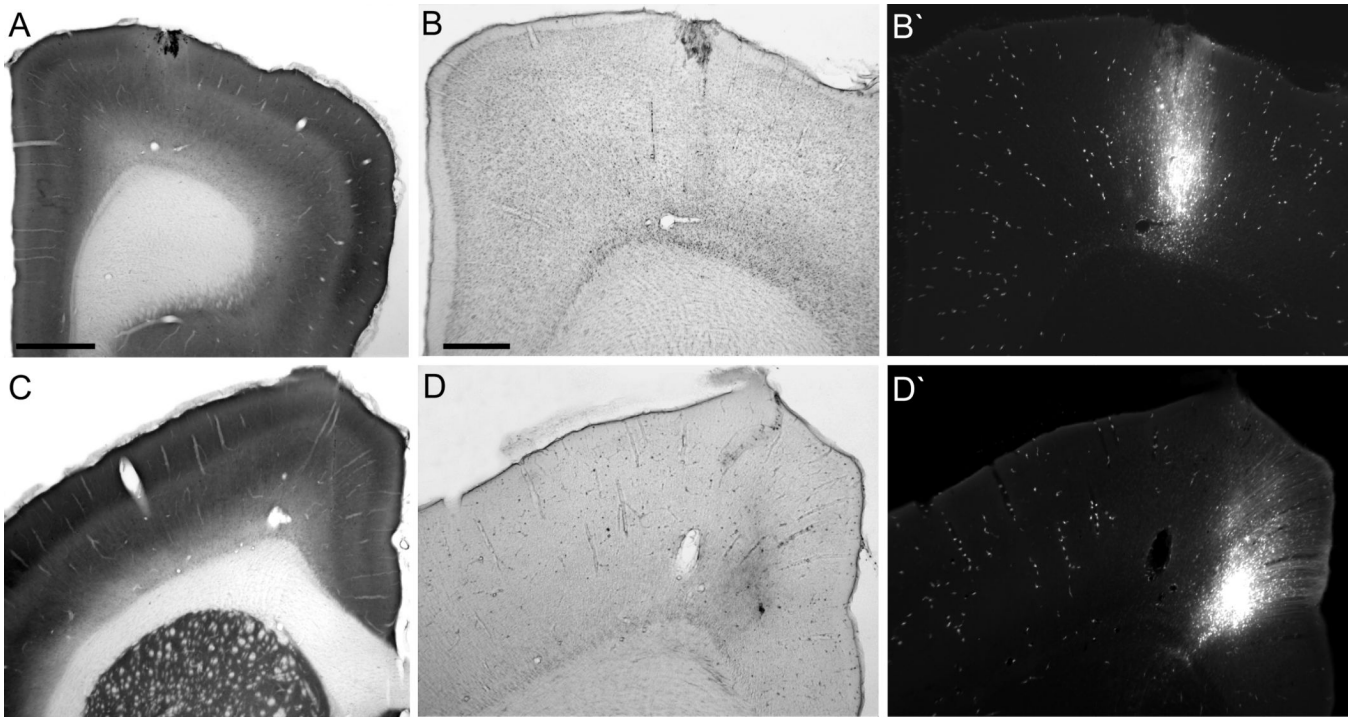

Fig. 2.

Examples of FR injections into the MI whisker and MI forepaw regions. **A:** Section through the MI forepaw region of case BN51 processed for cytochrome oxidase (CO). **B:** Adjacent unstained section through the FR injection site of BN51. **B`:** Same section in panel B visualized with fluorescent microscopy. **C:** Section through the MI whisker region of case BN53 processed for CO. **D:** Adjacent unstained section through the FR injection site of BN53. **D`:** Same section in panel D visualized with fluorescent microscopy. Scale bars = 1.0 mm in A (applies to C), 500 μm in B (applies to B`, D, D`).

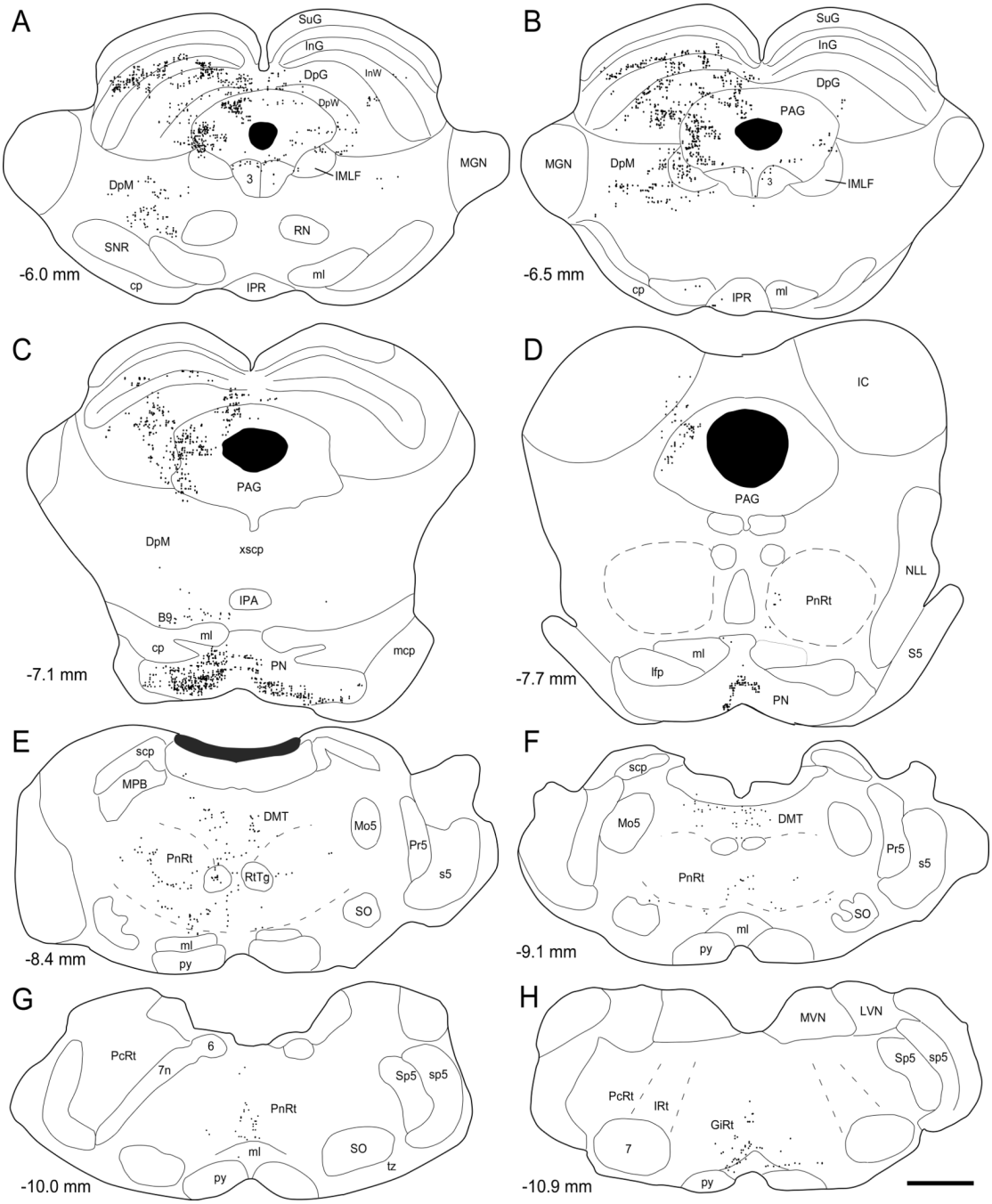

Fig. 3.

Bilateral distribution of FR-labeled varicosities in reconstructions of selected sections through the brainstem of MI whisker case BN53. Distance from bregma appears in the lower left of each plotted reconstruction. Scale, 1 mm.

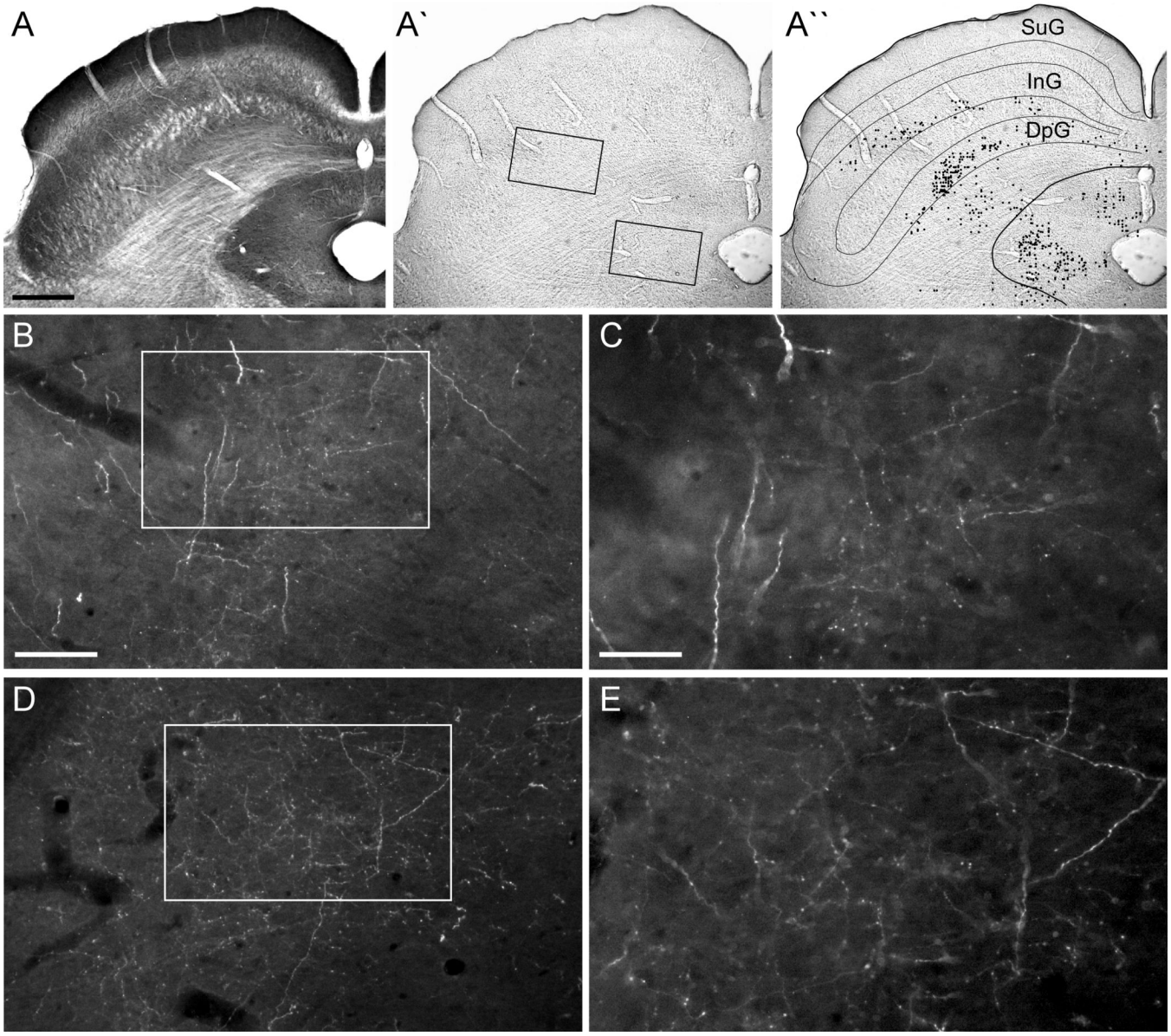

Fig. 4.

MI whisker projections to the ipsilateral superior colliculus (SC) and periaqueductal gray (PAG) in case BN53. **A:** Section through SC and PAG processed for CO. **A`:** Adjacent section (6.72 mm caudal to bregma) used for plotting labeled varicosities in SC and PAG; boxes indicate the regions in panels B and D. **A``:** Plot of labeled varicosities superimposed on the section in panel A`. **B,C:** Photomicrographs of FR-labeled terminals in the deep gray layer of the SC; box in panel B indicates the region in panel C. **D,E:** Photomicrographs of FR-labeled terminals in the PAG; box in panel D indicates the region in panel E. Scale bars = 1.0 mm in A (applies to A`, A``); 100 μm in B (applies to D), 50 μm in C (applies to E).

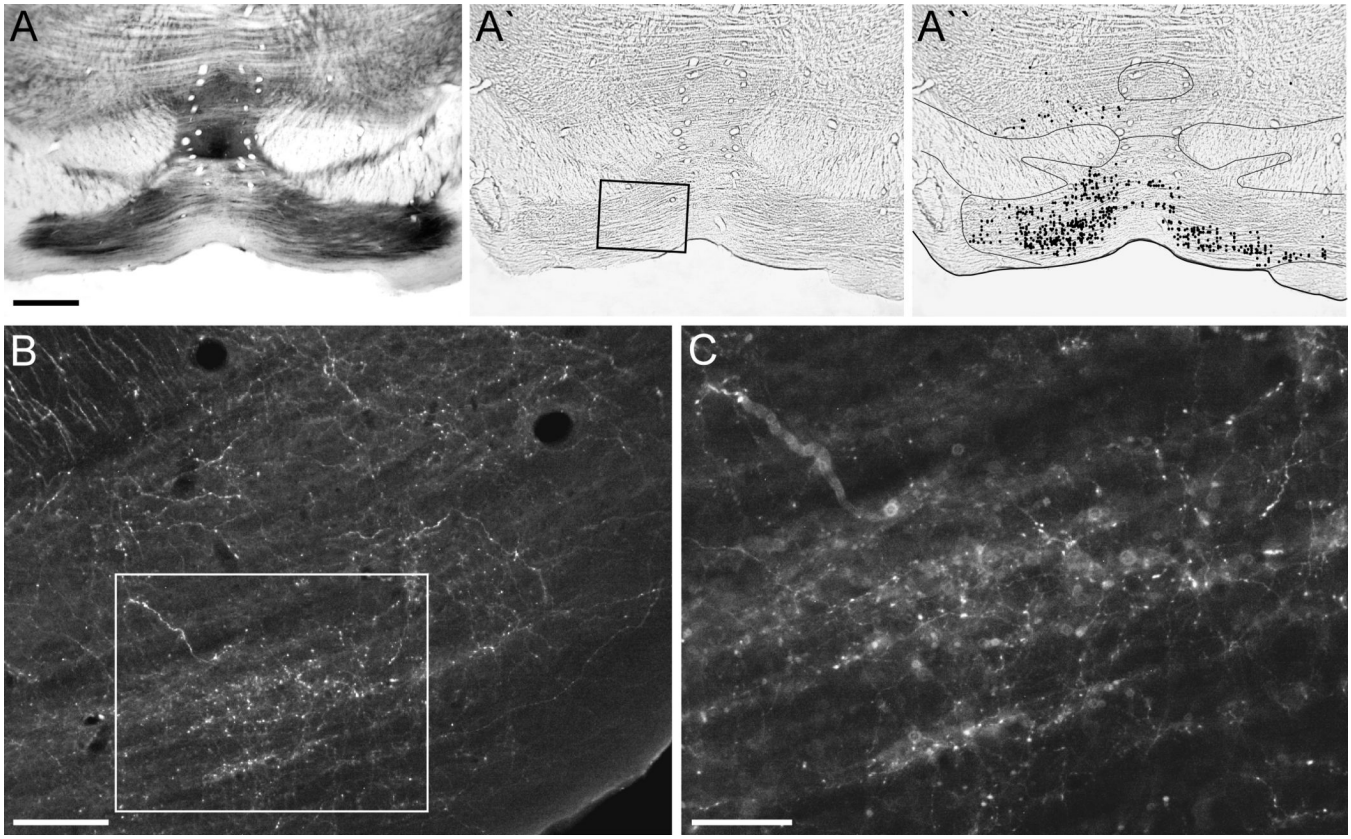

Fig. 5.

Bilateral MI whisker projections to the basal pons in case BN53. **A:** Section through the pons processed for CO. **A`:** Adjacent section (7.1 mm caudal to bregma) used for plotting labeled varicosities; box indicates the region in panel B. **A``:** Plot of labeled varicosities superimposed on the section in panel A`. **B,C:** Microscopic views of FR-labeled terminals in the basal pons; box in panel B indicates the region in panel C. Scale bars = 1.0 mm in A (applies to A`, A``); 100 μm in B, 50 μm in C.

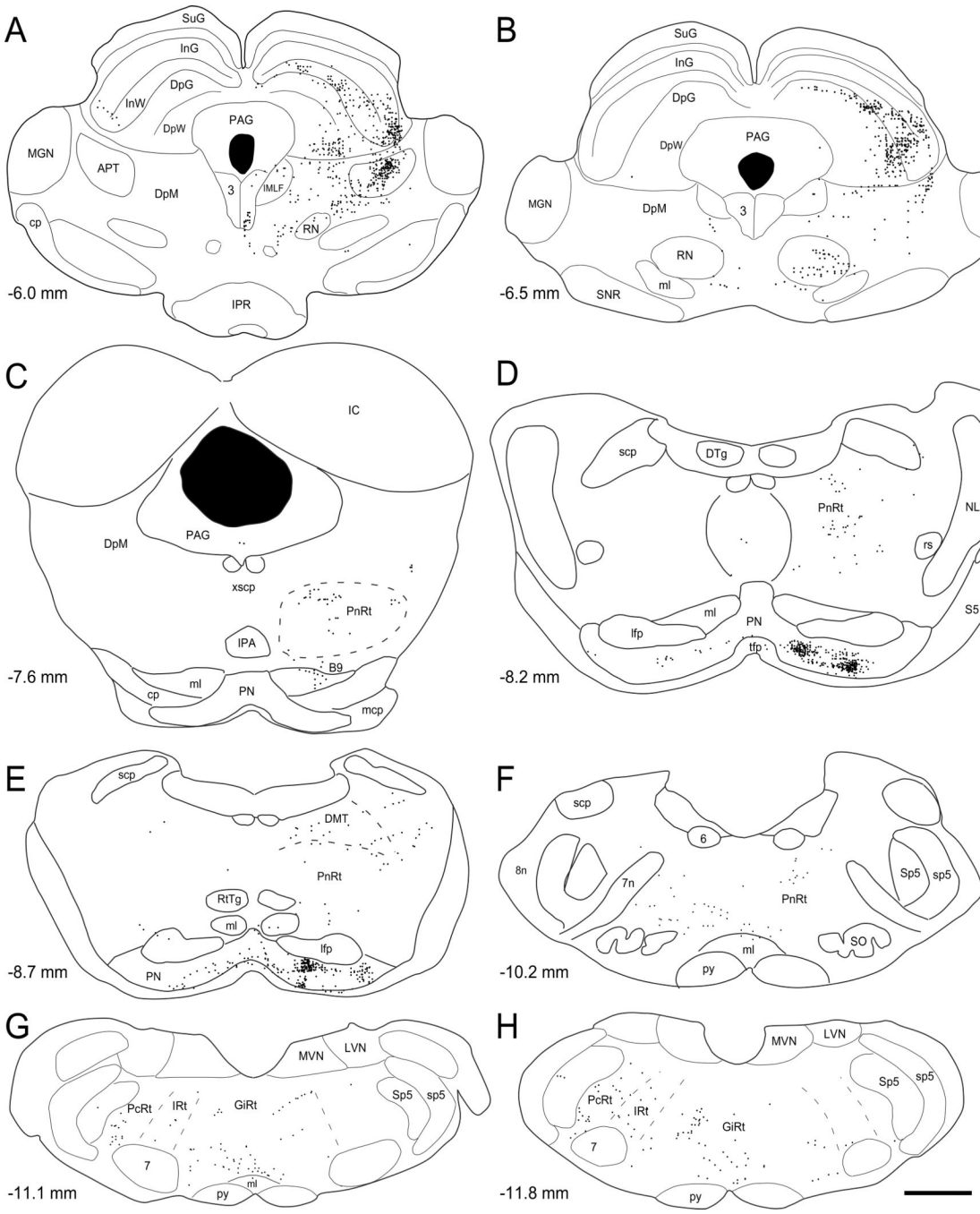

Fig. 6.

Bilateral distribution of FR-labeled varicosities in reconstructions of selected sections through the brainstem of MI forepaw case BN51. Distance from bregma appears in the lower left of each plotted reconstruction. Scale, 1 mm.

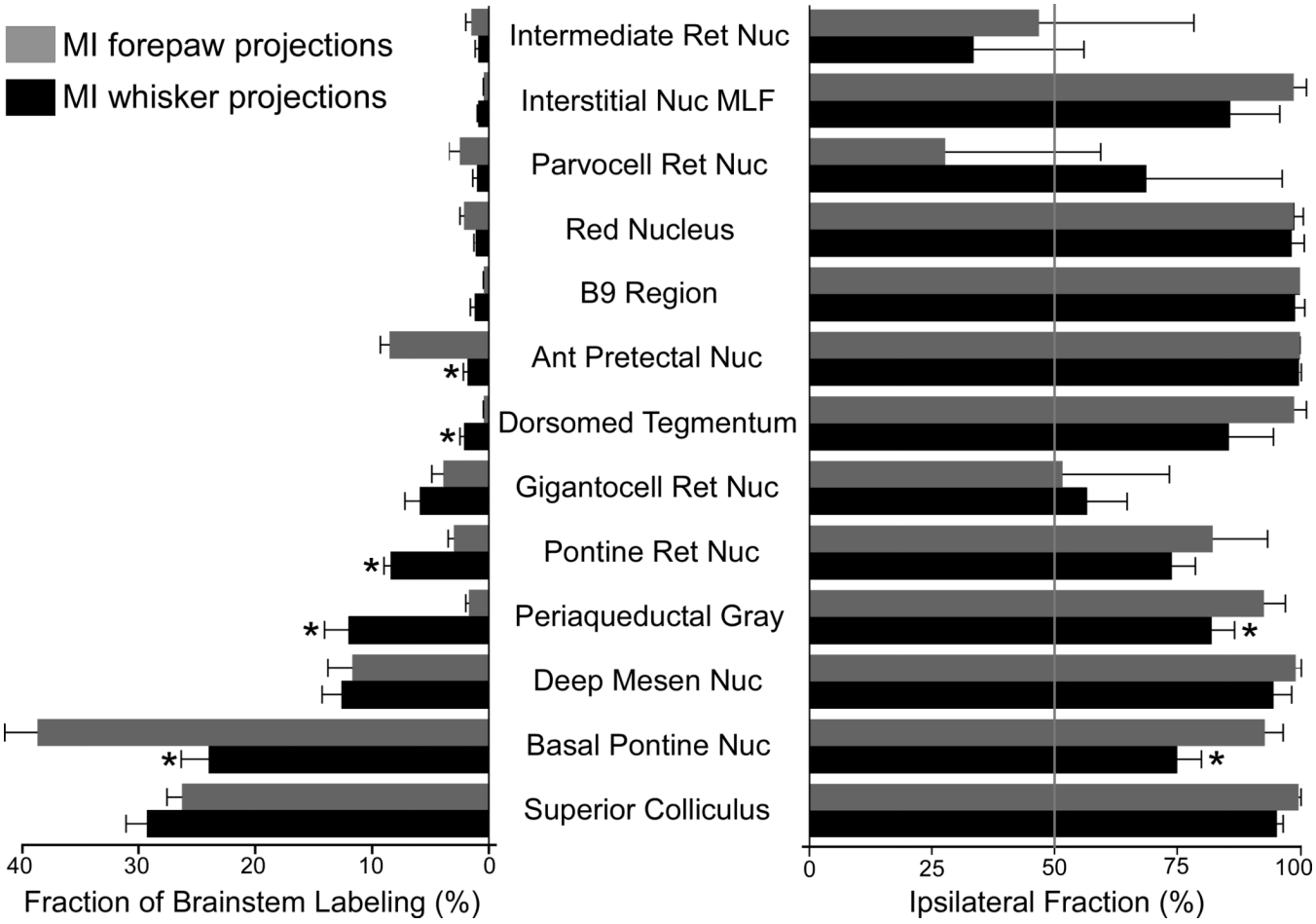

Fig. 7.

Regional distribution of MI projections to the brainstem. Left bargraph represents the normalized distribution of plotted varicosities in the brainstem structures listed in the center of the figure. Each bar represents the mean fraction of the sum of the plotted varicosities in the listed structures, based on FR injections in 8 rats for each group. Right bargraph indicates the mean proportion of plotted varicosities in each structure that appeared ipsilateral to the injection site. Bars lower than 50% indicate brain regions where the majority of varicosities were located contralateral to the FR injection. Brackets represent SEM; asterisks indicate significant differences between MI whisker and forepaw injections ($p < 0.01$; Student t-test).

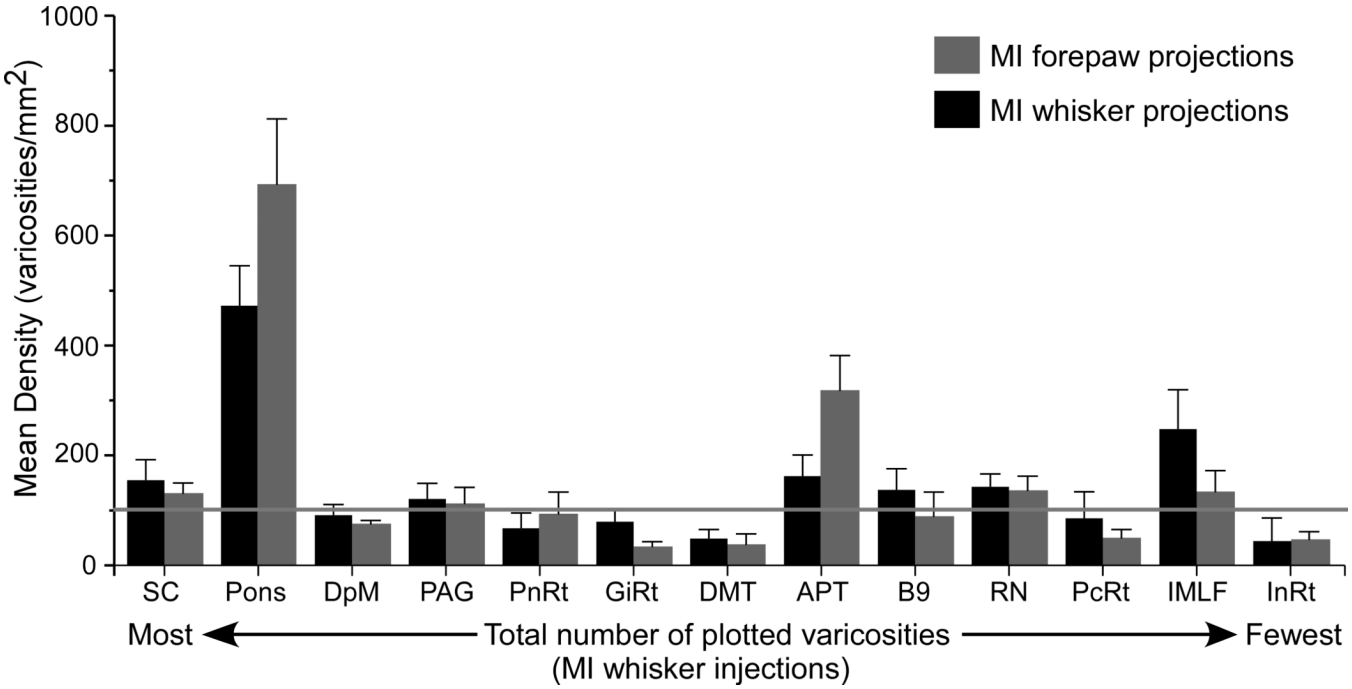

Fig. 8.

Mean density of plotted varicosities in 13 brainstem regions. Each bar represents the mean density from 8 cases for the side of the brainstem (usually ipsilateral) that contained the majority of plotted varicosities. Brain regions are ordered according to the total number of plotted varicosities as shown in Figure 7. Horizontal line indicates median density; brackets indicate SEM.

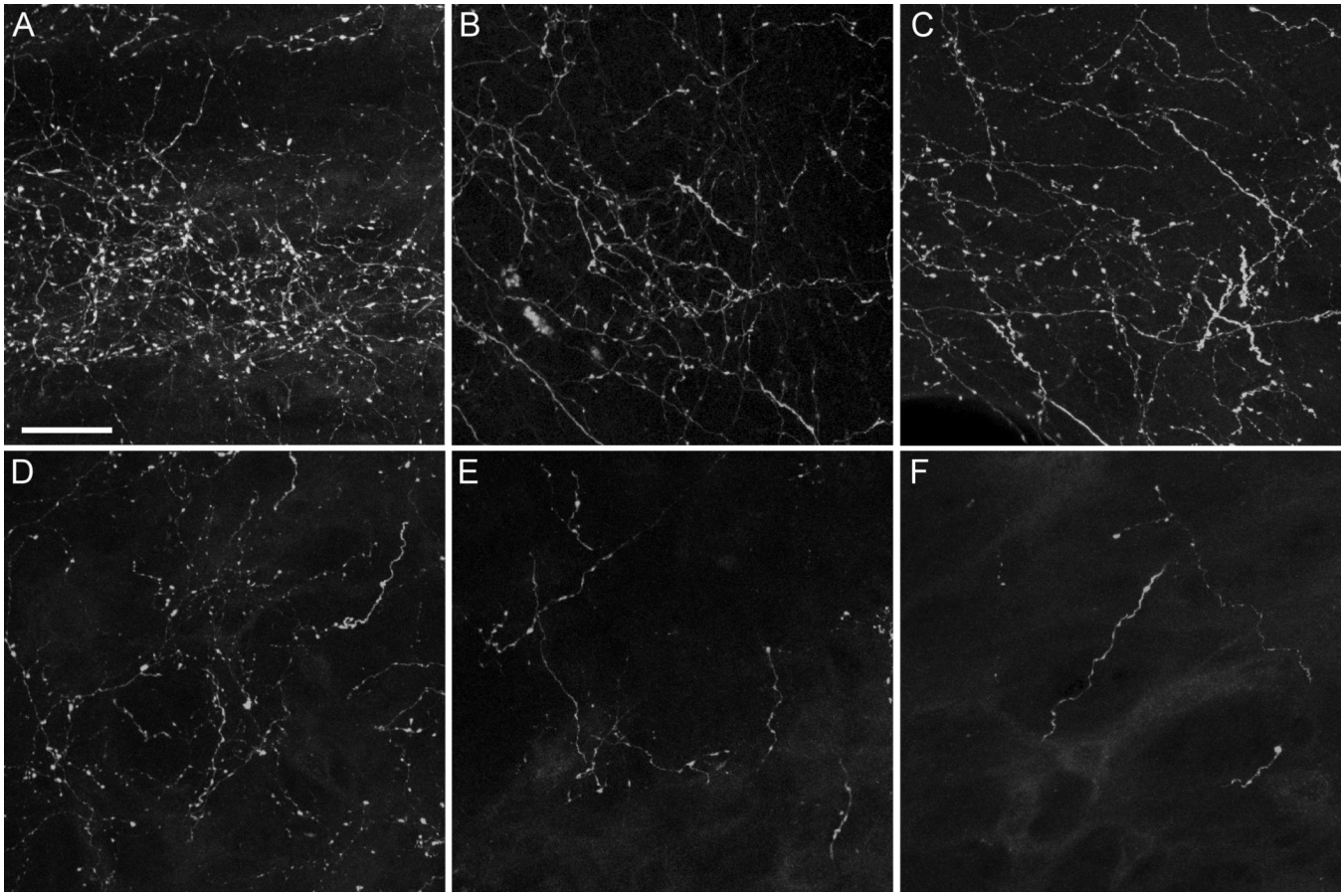

Fig. 9.

Confocal images of the densest terminal labeling in the brainstem regions that contained the largest number of plotted varicosities. Images were obtained either from BN53 or BN45, both of which received FR injections in the MI whisker region. **A:** Basal pons. **B:** Superior colliculus. **C:** Periaqueductal gray region **D:** Deep mesencephalic nucleus. **E:** Pontine reticular nucleus. **F:** Gigantocellular reticular nucleus. Scale, 25 μm.

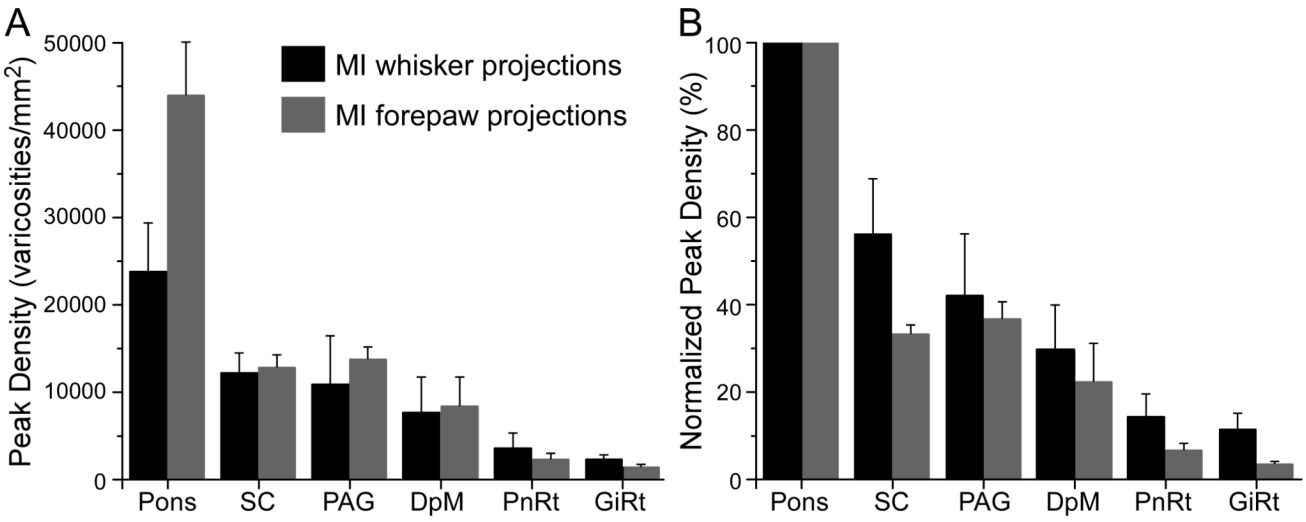

Fig 10.

Peak density of labeled varicosities in the brainstem regions that received the most projections from the whisker and forepaw regions in MI. **A:** Absolute peak density. **B:** Normalized peak density. The region with the highest density is defined as 100% and the other 5 regions are represented proportionate to that amount. Each bar represents the mean of 3 cases; brackets represent SEM.

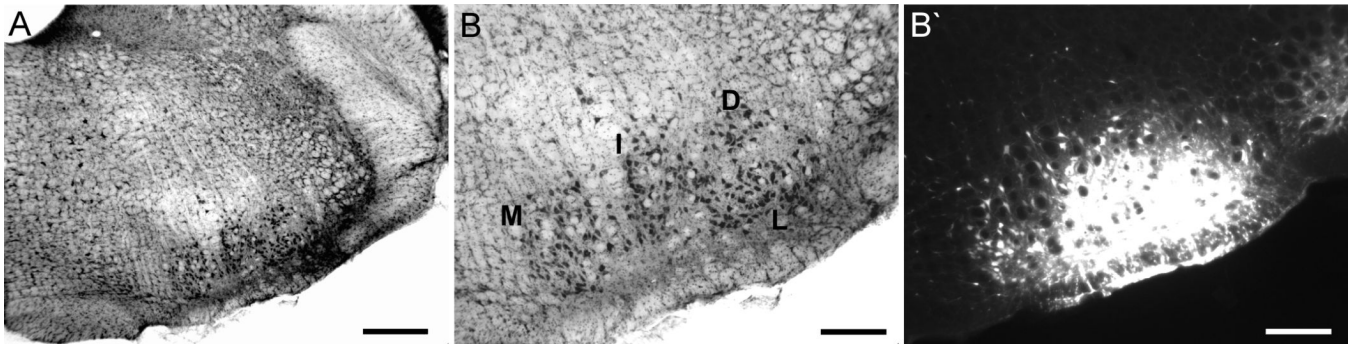

Fig. 11.

Retrograde tracer injection into the facial nucleus. **A:** Thionin-stained section through the facial nucleus. **B:** Magnified view of the facial nucleus illustrating the medial (M), intermediate (I), dorsal (D), and lateral (L) subnuclei. **B`:** Adjacent section using fluorescent microscopy to reveal the Fluoro-Gold (FG) injection into the lateral facial nucleus. Note that the FG also diffused into the intermediate subnucleus. Scale bars = 500 μm in A; 250 μm in B,B`.

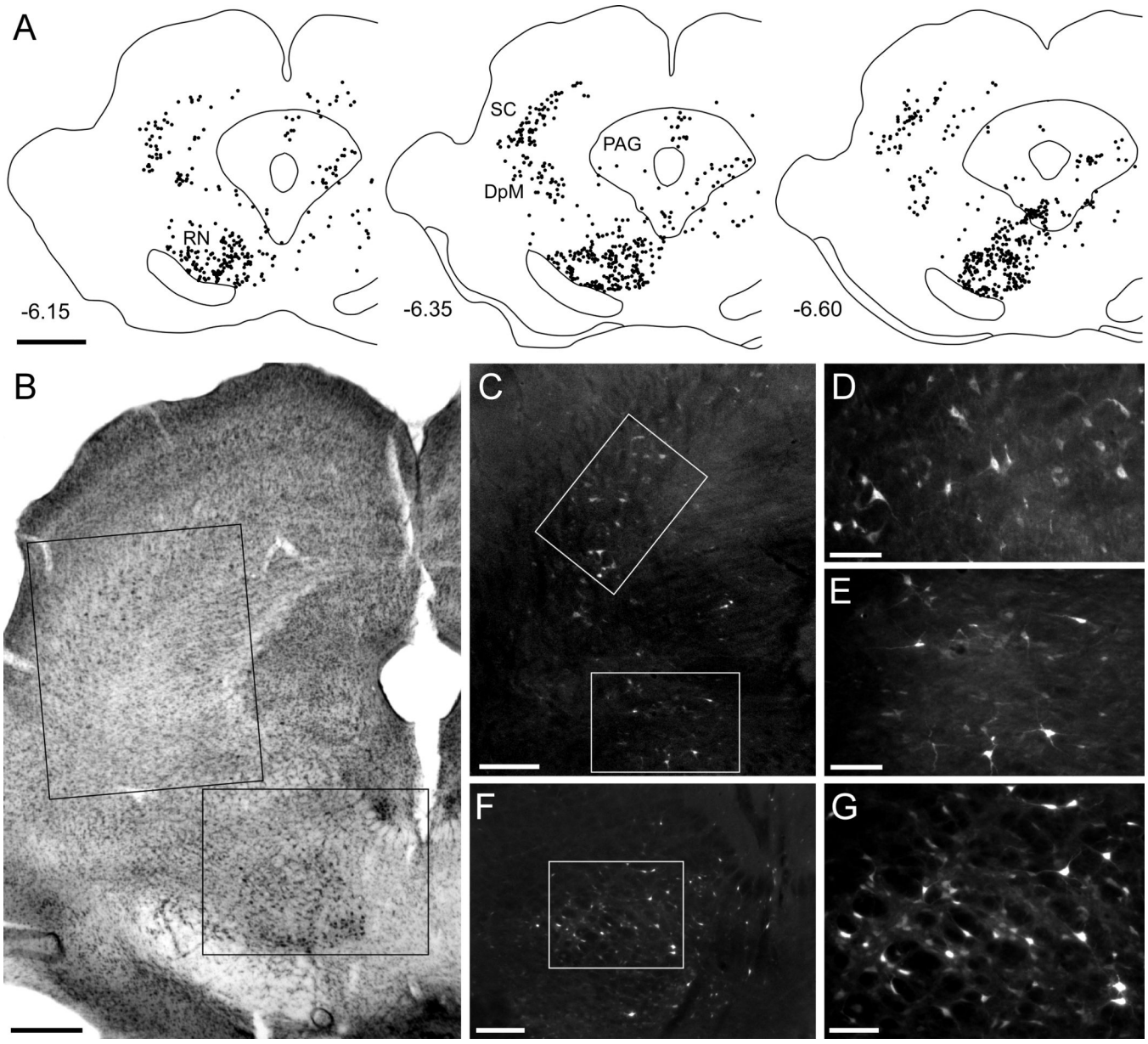

Fig. 12.

Midbrain neuronal labeling produced by the tracer injection in Figure 11. **A:** Reconstructed sections showing the distribution of FG-labeled neurons in the SC, PAG, DpM, and RN. Distance from bregma appears in the lower left of each plotted reconstruction. **B:** Thionin-stained section through the midbrain. Rectangles indicate approximate regions shown in panels C and F. **C:** Low power fluorescent microscopy showing FG-labeled neurons in SC and DpM. Rectangles indicate panels D and E. **D:** Labeled neurons in the deep gray layer of SC. **E:** Labeled neurons in the DpM. **F:** Low power fluorescent microscopy showing FG-labeled neurons in the RN. Rectangle indicates panel G. **G:** Labeled neurons in the RN. Scale bars = 1 mm in A; 500 μm in B; 250 μm in C and F; 100 μm in D, E, and G.

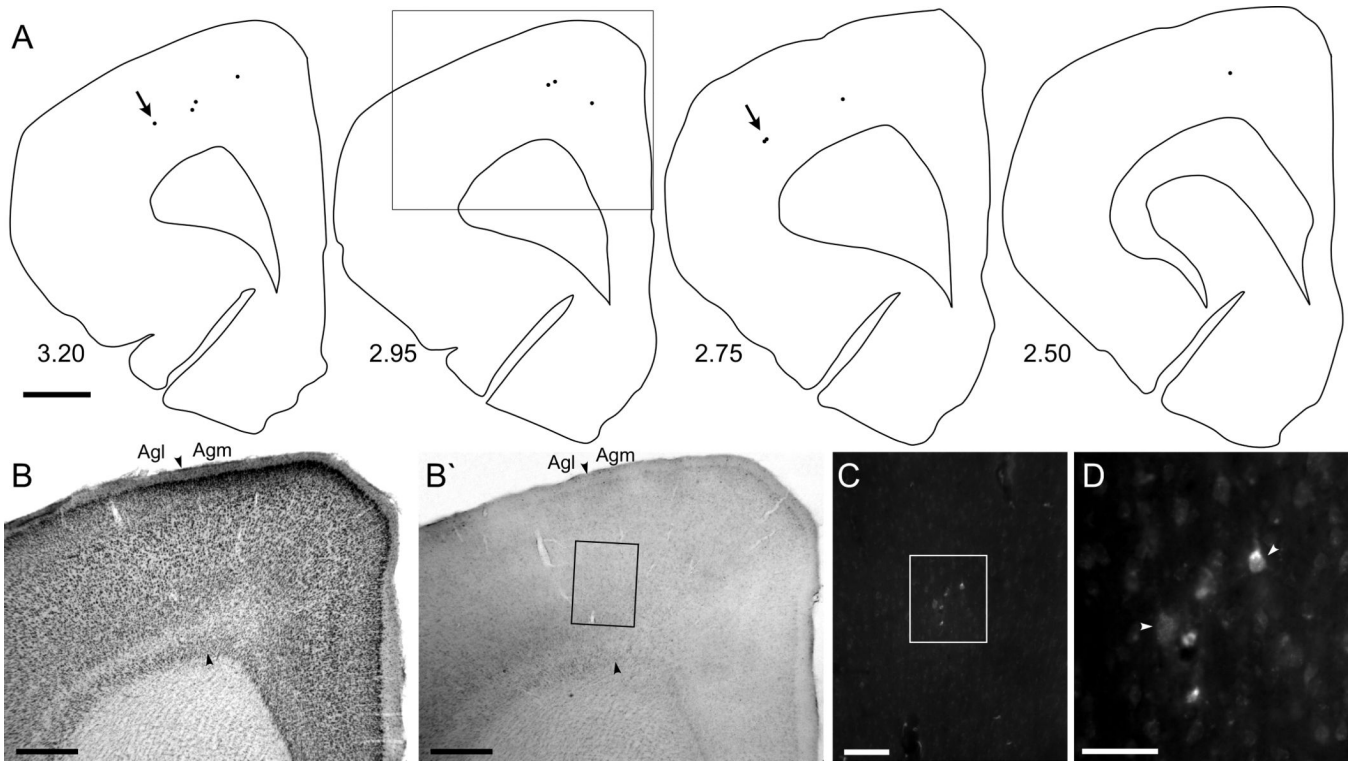

Fig. 13.

Neuronal labeling in MI cortex produced by the tracer injection in Figure 11. **A:** Reconstructions of FG-labeled neurons in MI. Distance from bregma appears in the lower left of each plotted reconstruction;.arrows indicate lateral neurons likely to be in the jaw, lip, and tongue representations. Box represents region in panels B and B`. **B, B`:** Adjacent sections through MI used for conventional (B) and fluorescent (B`) microscopy. Rectangle in B` indicates the region in panel C. **C:** Pair of FG-labeled neurons near the border between Agl and Agm. Rectangle indicates the region in panel D. **D:** Magnified view of two FG-labeled neurons as indicated by arrowheads; one was brightly-lit while the other was only faintly-labeled. Scale bars = 1 mm in A; 500 μm in B,B`; 200 μm in C; 50 μm in D.

TABLE 1

Summary of Fluoro-Ruby Injections in MI Cortex

Case	Injection Volume	MI Cortical Region[1]
BN12	120 nl	Right Agm - Wh
BN16	142 nl	Right Agl - Fp
BN23	120 nl	Right Agl - Fp
BN25	102 nl	Right Agm - Wh
BN28	120 nl	Right Agl - Fp
BN33	120 nl	Right Agl - Fp
BN37	150 nl	Right Agm - Wh
BN38	150 nl	Right Agm - Wh
BN39	150 nl	Right Agm - Wh
BN40	150 nl	Right Agl - Fp
BN41	150 nl	Right Agl - Fp
BN45	150 nl	Right Agm - Wh
BN49	120 nl	Left Agm - Wh
BN51	120 nl	Right Agl - Fp
BN53	105 nl	Left Agm - Wh
BN54	100 nl	Right Agl - Fp

Agm-Wh, medial agranular, whisker; Agl-Fp, lateral agranular, forepaw